Journal of Marine Research, 72, 183–218, 2014

Group behavior among model bacteria influences particulate carbon remineralization depths

by K. A. S. Mislan[1,2], Charles A. Stock[3], John P. Dunne[3], and Jorge L. Sarmiento[1]

ABSTRACT

Organic particles sinking from the sunlit surface are oases of food for heterotrophic bacteria living in the deep ocean. Particle-attached bacteria need to solubilize particles, so they produce exoenzymes that cleave bonds to make molecules small enough to be transported through bacterial cell walls. Releasing exoenzymes, which have an energetic cost, to the external environment is risky because there is no guarantee that products of exoenzyme activity, called hydrolysate, will diffuse to the particle-attached bacterium that produced the exoenzymes. Strategies used by particle-attached bacteria to counteract diffusive losses of exoenzymes and hydrolysate are investigated in a water column model. We find that production of exoenzymes by particle-attached bacteria is only energetically worthwhile at high bacterial abundances. Quorum sensing provides the means to determine local abundances, and thus the model results support lab and field studies which found that particle-attached bacteria have the ability to use quorum sensing. Additional model results are that particle-attached bacterial production is sensitive to diffusion of hydrolysate from the particle and is enhanced by as much as 15 times when diffusion of exoenzymes and hydrolysate from particles is reduced by barriers of biofilms and particle-attached bacteria. Bacterial colonization rates and activities on particles in both the euphotic and mesopelagic zones impact remineralization length scales. Shoaling or deepening of the remineralization depth has been shown to exert significant influence on the residence time and concentration of carbon in the atmosphere and ocean. By linking variability in remineralization depths to mechanisms governing bacterial colonization of particles and group coordination of exoenzyme production using a model, we quantitatively connect microscale bacteria-particle interactions to the carbon cycle and provide new insights for future observations.

1. Introduction

The global air-sea CO_2 balance is sensitive to attenuation of sinking particulate organic carbon with depth in the ocean (Kwon, Primeau, and Sarmiento 2009) and has a high degree of mechanistic uncertainty (Buesseler et al. 2007) and regional variability (Lutz, Dunbar, and Caldeira 2002). More atmospheric CO_2 is absorbed into the ocean when particles transport organic carbon deeper, on a scale of 10s of meters, because ventilation of deeper water

1. Atmospheric and Oceanic Sciences Program, Princeton University, 300 Forrestal Road, Princeton, NJ 08544.
2. Corresponding author ***e-mail: kas.mislan@gmail.com***
3. NOAA Geophysical Fluid Dynamics Laboratory, 201 Forrestal Road, Princeton, NJ 08540.

occurs over longer timescales (Kwon, Primeau, and Sarmiento 2009). Organisms influence CO_2 distribution by consuming most of the organic carbon from sinking particles in the mesopelagic zone and transforming it to CO_2 through respiration (reviewed by Herndl and Reinthaler 2013). If the carbon budget is balanced in the mesopelagic zone, bacteria respire most of the sinking organic carbon (Giering et al. 2014). Global biogeochemical models that predict the climate impacts of anthropogenic CO_2 emissions parameterize the remineralization of sinking particles using measurements from sediment traps but exclude many biological mechanisms, such as bacterial activity, that may be critical for determining how deep organic carbon sinks before it is utilized by organisms in the mesopelagic zone. Considering the sensitivity to this parameter as shown by Kwon, Primeau, and Sarmiento (2009), more mechanistic parameterizations that include biological processes may be necessary to capture the variability in remineralization of sinking particles.

Many different strains of bacteria colonize particles (Jing et al. 2012), and the particles themselves are diverse in physical structure and nutrient composition (Bishop et al. 1977; Alldredge 1979). The essential nutrients in particles may be remote from the locations of bacteria, creating a set of circumstances where production of exoenzymes may enhance their ability to access nutrients (Vetter et al. 1998). Exoenzyme activity rapidly solubilizes nutrients in particles (Smith et al. 1992), and growth rates of particle-attached bacteria are enhanced relative to free-living bacteria (Karner and Herndl 1992; Smith et al. 1992; Müller-Niklas et al. 1994). Exoenzymes diffuse out of particles into the dissolved environment (Ziervogel et al. 2010) and are present in high enough concentrations to be measured along ocean transects (Baltar et al. 2009, 2010).

Vetter et al. (1998) modeled a single bacterium in a particle and determined that due to the rapid diffusion rates of exoenzymes and solubilized nutrients, a single bacterium was unlikely to energetically benefit from producing exoenzymes. In their conclusions, they hypothesized that a bacterium would be more likely to benefit energetically if exoenzymes are produced by bacterial consortia and/or if bacteria employ mechanisms to reduce diffusive losses from particles. There is recent evidence from field and lab studies that these mechanisms are indeed important. Bacteria coordinate behavior among individuals by using signaling molecules that regulate gene expression in a process called quorum sensing (Miller and Bassler 2001). Bacterial strains isolated from marine snow particles produce quorum-sensing signal molecules (Gram et al. 2002). Quorum-sensing signal molecules stimulate exoenzyme activity within marine particles and have been found in marine particles collected from sediment traps (Hmelo, Mincer, and Van Mooy 2011). Diffusive losses decrease when bacteria produce biofilms that retain exoenzymes and hydrolysate (Drescher et al. 2014).

A primary goal of this study was to link together these critical mechanisms to create a water column model of sinking particles, hereafter referred to as the microbial remineralization model. The microbial remineralization model simulates biogeochemical consequences and therefore serves as an alternative to the more empirical methods currently used to predict attenuation of particles in the ocean water column of global models. We then conducted a series of sensitivity experiments using the model to determine the effect of bacterial behavior

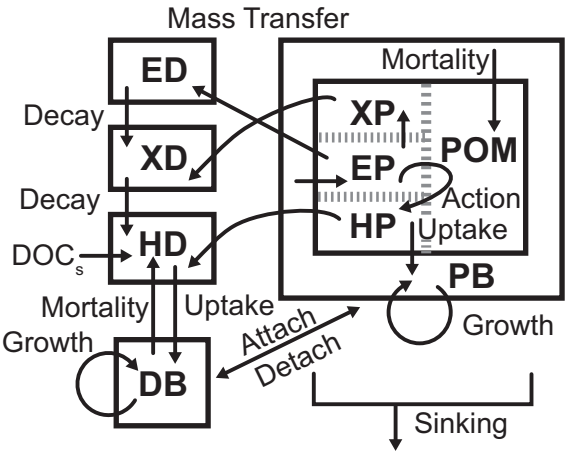

Figure 1. Diagram of the microbial remineralization model. POM is particulate organic matter. PB is particle-attached bacteria. DB is free-living bacteria. EP is active exoenzyme in the particle. HP is hydrolysate in the particle. XP is inactive exoenzyme in the particle. ED is active exoenzyme in the dissolved environment. HD is hydrolysate in the dissolved environment. XD is inactive exoenzyme in the dissolved environment. Semilabile dissolved organic carbon, DOC_s, in the water column decays with a turnover time of 5 years into hydrolysate in the dissolved environment, HD. The environment is distinguished by one of the letters of the state variable; D is dissolved, and P is particle. The units for all the state variables are mg C m^{-3} seawater.

and abundance on bacterial production and carbon flux profiles in the ocean water column. Vetter et al. (1998) demonstrated the importance of diffusion, so one set of sensitivity studies simulated the effect of bacterial uptake in particles relative to diffusion. The effect of the retention of solubilized nutrients and exoenzymes in particles was also included. Another set of sensitivity experiments assessed the effect of variations in particle-attached bacterial abundance at the base of the euphotic zone on carbon flux in the mesopelagic zone.

2. Methods

a. Model description

The microbial remineralization model explicitly describes the interactions between sinking particles and heterotrophic bacteria using nine state variables associated with two physical environments, dissolved and particulate, in a one-dimensional Eulerian framework. The model has a vertical range from the base of the euphotic zone to the ocean bottom. (See Fig. 1 for a diagram of the model.) The model is based on process-based experimental studies: Free-living bacteria colonize sinking particles, a rich source of nutrients, becoming particle-attached bacteria (Kiørboe et al. 2002). Particles are too big for bacteria to consume directly, so particle-attached bacteria release exoenzymes, which cleave small molecules, hydrolysate, from the larger particle (Arnosti 2011). Exoenzyme is active for a

limited period of time before it becomes inactive (Steen and Arnosti 2011). Hydrolysate is either consumed by the particle-attached bacteria or transferred outside the particle through a combination of advection and diffusion (Kiørboe, Ploug, and Thygesen 2001). Outside the particle, hydrolysate is available for consumption by free-living bacteria. Exoenzyme, active and inactive, is also transferred to the dissolved environment (Ziervogel et al. 2010), where it decays to hydrolysate. Particle-attached bacteria detach from the particle becoming free-living bacteria (Kiørboe et al. 2002, 2003). Free-living bacteria are inhibited from attaching to particles when high particle-attached bacterial abundances increase competitive interactions among bacteria (Grossart et al. 2003).

A key trade-off incorporated into the model is between particle-attached bacterial growth and exoenzyme production. Equation (1) determines the change in particle-attached bacterial, PB, concentration per time step and is a combination of growth, μ_{PB}; colonization β; detachment, δ; mortality, m_{PB}; and sinking, w. DB is the concentration of free-living bacteria.

$$\frac{d\mathrm{PB}}{dt} = \mu_{\mathrm{PB}}\mathrm{PB} + \beta\mathrm{DB} - \delta\mathrm{PB} - m_{\mathrm{PB}}\mathrm{PB}^{2} + w\frac{d\mathrm{PB}}{dz} \tag{1}$$

Equation (2) calculates μ_{PB}, growth of particle-attached bacteria, and includes a term for exoenzymes, ϵ in units of h^{-1},

$$\mu_{\mathrm{PB}} = B_{GEmax}v_{\mathrm{PB}} - \Upsilon - \epsilon \tag{2}$$

where Υ is the basal metabolic rate constant (h^{-1}), B_{GEmax} is the bacterial growth efficiency (dimensionless), and v_{PB} is nutrient uptake (h^{-1}). A full description of the model is given in the Appendix and the parameters are in Table A1.

The following simplifications were made in the model for the analyses presented herein: Particles are a single size and spherical. Leucine aminopeptidase was chosen to represent the characteristic exoenzyme activity rates because leucine aminopeptidase is typically one of the most prevalent exoenzymes measured in particles (Arnosti 2011). Different types of exoenzymes have different activity rates (Steen and Arnosti 2011), which is why the specification is important. For comparison, leucine aminopeptidase has an activity rate of 118 h^{-1} whereas β-glucosidase has an activity rate of 8.6 h^{-1} (Steen and Arnosti 2011). Particle-attached bacteria in the model are restricted to using exoenzymes that freely diffuse and adsorb to substrates away from the particle-attached bacteria to solubilize particulate organic carbon in particles (Hoppe, Arnosti, and Herndl 2002; Azam and Malfatti 2007). Freely dissolved exoenzymes are frequently >50% and up to 100% of total activity (Baltar et al. 2010; Duhamel, Dyhrman, and Karl 2010), particularly below 100 m depth (Baltar et al. 2013). These simplifications enable an initial analysis of the nature and importance of interactions between the diverse processes in the model. Ballast minerals, calcium carbonate, opal, and lithogenic material are included in the model as components of the particle structure (Armstrong et al. 2002; Klaas and Archer 2002). As an additional simplification

in the model, the ballast minerals maintain the size and sinking speed of the particles as the organic carbon is solubilized.

b. Diffusion dynamics

The rate of hydrolysate diffusion out of particles has implications for the uptake of hydrolysate by particle-attached bacteria (Vetter et al. 1998). Particle-attached bacterial uptake and diffusion can either be modeled as two distinct losses of hydrolysate, or particle-attached bacterial uptake can be from the diffusive loss of hydrolysate. An example of particle-attached bacterial uptake from the diffusive loss is that bacteria near the surface of a particle intercept hydrolysate as it diffuses out of the particle before it is lost to the surrounding water (Kiørboe, Ploug, and Thygesen 2001). It is also possible that particle-attached bacteria slow diffusion of hydrolysate and exoenzymes out of particles by using biofilms (Hannides, Dunn, and Aller 2005; Drescher et al. 2014). The model was used to explore the effects of these processes on particle-attached bacterial production. The following scenarios were used: (1) *Interior*, in which particle-attached bacterial uptake and diffusion are modeled as separate losses; (2) *Interception*, in which particle-attached bacteria take up hydrolysate as it is diffusing from the particle; and (3) *Retention*, in which particle-attached bacteria retain hydrolysate and prevent it from diffusing outside of the particle. In the *Retention* scenario, active and inactive exoenzyme are also retained in the particle by bacteria but are still are able to diffuse small distances. Inactive exoenzyme is exoenzyme that is degraded and can no longer adsorb to substrates (Steen and Arnosti 2011). *Interior, Interception, and Retention* are simplifications designed to assess the energetic and biogeochemical implications of diffusion of exoenzymes and hydrolysate out of particles in the model. The Appendix has detailed descriptions of how bacterial uptake, diffusion, and retention are incorporated into the model equations.

c. Exoenzyme production

Bacteria are known to coordinate exoenzyme production by using quorum-sensing signal molecules (Hmelo, Mincer, and Van Mooy 2011), but there are many unknowns in how quorum sensing results in the production of exoenzymes in particles. Therefore, instead of imposing the properties of exoenzyme production for each of the configurations described previously, we carry out sensitivity studies with the model to determine the optimal exoenzyme production as a function of attached bacterial abundance. A representative particle was initialized with particle-attached bacterial abundances between 2.51×10^5 and 2.76×10^7. For each particle-attached bacterial abundance value, the biomass-specific exoenzyme production rate was varied between 0 and 0.05 h^{-1}. Nutrients used to generate these exoenzymes cannot be used for growth, presenting a trade-off between immediate growth versus investment in the potential for future growth (equation 2). When the exoenzyme production rate exceeds the growth rate, then exoenzymes are produced at the expense of particle-attached bacterial biomass.

At the start of the model simulations, concentrations of exoenzyme and hydrolysate were zero. The system was allowed to "spin-up" for 3 h, long enough to allow available hydrolysate to reflect the exoenzyme production rate but short enough that the particle-attached bacterial abundance did not diverge substantially from the initial condition. It was necessary to keep the particle-attached bacterial abundance close to the initial condition in order to associate an optimal exoenzyme production rate with each initial biomass of particle-attached bacteria. For similar reasons, bacterial attachment and detachment were omitted to isolate the exoenzyme production value producing the maximum growth of the initial particle-attached bacterial population. After the "spin-up," production of particle-attached bacteria over the residence time (defined as total inventory/loss rate) of exoenzyme within the particle (~9 min), was then calculated. The exoenzyme production rate yielding the highest particle-attached bacterial production was taken as the optimal rate for each initial biomass of particle-attached bacteria.

d. Carbon flux

The effect of particle-attached bacterial group behavior on carbon flux in the water column was determined for the Bermuda Atlantic Time Series (BATS) station in the North Atlantic subtropical gyre. The average particle flux, 27.8 mg C m^{-2} d^{-1}, from the monthly sediment trap deployments (1990–2010) at 150 m was used to force the model. Carbon flux was calculated as the combined flux of particulate organic matter and particle-attached bacteria in order to be consistent with measurements from sediment traps. The model results were compared with 200 and 300 m traps from the BATS station and 500, 1,500, and 3,200 m traps from the Oceanic Flux Program (OFP), which are in close proximity to the BATS station. The BATS station 200 and 300 m trap data used in the comparison are averages from a subset ($n = 19$ trap deployments) when 150 m trap collections were within 27.8 ± 1 mg m^{-2} d^{-1}. Long-term averages from the moored OFP traps, which were deeper and less variable, were used (Conte, Ralph, and Ross 2001). A power law fit to the sediment trap data was calculated using the method of Martin et al. (1987) to provide an additional diagnostic for comparison that is similar to curves used in global biogeochemical models to represent particulate carbon remineralization (Martin et al. 1987).

Particles fluxing into the mesopelagic zone likely have a seed of particle-attached bacteria from colonization that takes place in the euphotic zone or, in the case of fecal pellets, in the guts of animals (Nagasawa and Nemoto 1988). We reference particle-attached bacterial abundance relative to particle surface area because particle surface area is used to determine colonization rates of particles (Kiørboe et al. 2002). The area of bacterial coverage of the particle was calculated by assuming that all particle-attached bacteria are rod shaped with 1 μm length and 0.5 μm diameter, which equals a coverage area per particle-attached bacteria of 0.5 μm^2. The particles were assumed to be spherical, so the surface area was equal to $4\pi r^2$. The particles in the model had a radius r of 1 mm, so the surface area of each particle

was 12 mm^2. The surface area of the particle divided by the coverage area per particle-attached bacterium equals the particle-attached bacterial abundance for 100% coverage. We specified initial particle-attached bacterial populations of 6.3×10^6, 1.3×10^7, and 2.5×10^7 bacteria $particle^{-1}$ equivalent to 25%, 50%, and 100% bacterial coverage of the particle surface area to evaluate the sensitivity of the model to bacterial colonization that takes place in the euphotic zone.

e. Free-living bacteria

Particles supplement concentrations of free-living bacteria in the microbial remineralization model through three mechanisms. One mechanism is that hydrolysate transfers out of the particle, and free-living bacteria take up the dissolved hydrolysate, which is used for growth (Smith et al. 1992). A second mechanism is that particle-attached bacteria detach from the particles and become free-living bacteria (Kiørboe et al. 2002, 2003). In the microbial remineralization model, detachment is based on antagonistic interactions due to competition, so the rate is determined by the abundance of particle-attached bacteria. Therefore, both cooperation to produce exoenzymes and antagonistic interactions that cause detachment depend on particle-attached bacterial abundance. There are stages for these processes, which have importance for interpreting the microbial remineralization model results. At low abundances, particle-attached bacteria do not produce exoenzymes and do not detach. At medium abundances, particle-attached bacteria produce exoenzymes but do not detach. At high abundances, particle-attached bacteria produce exoenzymes and detach from particles. Last, the third mechanism by which particles supplement free-living bacterial concentration is that exoenzymes transfer out of the particle and decay with a 5-year turnover time to dissolved hydrolysate, which free-living bacteria take up and use for growth. In the model, exoenzymes have the same turnover time, 5 years, as measured for semilabile dissolved organic carbon (Abell, Emerson, and Renaud 2000), because specific turnover times for exoenzymes are not yet known. An additional source of dissolved hydrolysate that is unrelated to particles in the model is from the decay of semilabile dissolved organic carbon with a 5-year turnover time (DOC_s in Fig. 1) (Abell, Emerson, and Renaud 2000).

3. Results

a. Diffusion dynamics comparisons

The diffusion environment within the particles was analyzed by calculating the residence time (defined as total inventory/loss rate) of exoenzyme and hydrolysate (Jumars et al. 1989, 1993; Kiørboe, Ploug, and Thygesen 2001). For typical marine particles considered here (1 mm radius sinking 48 m d^{-1}), residence times of both hydrolysate (46 s) and exoenzyme (9 min) are very short, underpinning the importance of strategies to combat these losses. The effects of diffusion dynamics on bacteria in particles are represented by the *Interior*, *Interception*, and *Retention* scenarios (Fig. 2). The particle-attached bacterial production values at 20×10^6 bacteria $particle^{-1}$, 80% coverage, are quantitatively compared to illustrate

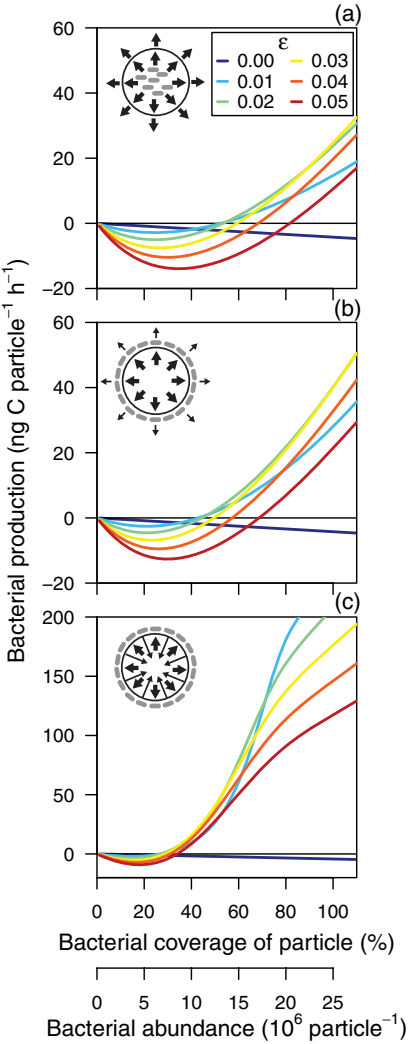

Figure 2. Particle-attached bacterial abundance and exoenzyme production rate influences particle-attached bacterial production. The scenarios modeled were the following: (a) *Interior*, in which particle-attached bacterial uptake and diffusion are modeled as separate losses; (b) *Interception*, in which particle-attached bacteria take up hydrolysate as it is diffusing from the particle; and (c) *Retention*, in which particle-attached bacteria retain hydrolysate and exoenzyme inside the particle. The bacterial and solute flux characteristics distinguishing *Interior*, *Interception*, and *Retention* are shown in diagrams in the upper left corner of each plot. The circle is the particle, the gray ovals are particle-attached bacteria, and the arrows indicate the direction of hydrolysate flux from the particle (large arrows indicate high hydrolysate flux, and small arrows indicate low hydrolysate flux). The modeled particles had a radius of 1 mm and a sinking rate of 48 m d^{-1}. The colored lines represent different values of ε, exoenzyme production rate, ranging from 0 to 0.05 h^{-1}.

the differences shown in Figure 2. The particle-attached bacterial production at 20×10^6 bacteria particle^{-1} for the *Interior*, *Interception*, and *Retention* scenarios are 11.7, 21.8, and 181.0 ng C particle^{-1} h^{-1} respectively (Fig. 2). The particle-attached bacterial production in the *Interception* and *Interior* scenarios is similar relative to the *Retention* scenario, which at 20×10^6 bacteria particle^{-1} was 15 times and 8 times the *Interior* and *Interception* scenarios respectively (Fig. 2). *Retention* of hydrolysate and exoenzyme within the particle greatly enhanced particle-attached bacterial production by minimizing losses from the particle to the dissolved environment.

There are also some similarities among the *Interior*, *Interception*, and *Retention* results (Fig. 2). One similarity is that at low particle-attached bacterial abundances, particle-attached bacterial production is less than zero (Fig. 2). Another similarity is that $\epsilon = 0.05$ h^{-1}, the maximum exoenzyme production rate constant in the analysis, results in the lowest particle-attached bacterial production at both low and high particle-attached bacterial abundances (Fig. 2). Both of these results are related to the relative energetic costs versus benefits of producing exoenzymes in the model (equation 2). At low particle-attached bacterial abundances in Figure 2, little exoenzyme is produced so little hydrolysate is generated for particle-attached bacteria to take up before the exoenzymes diffuse out of the particles. Therefore, producing no exoenzymes, $\epsilon = 0$, is the best strategy. The gradual decrease in particle-attached bacterial production when $\epsilon = 0$ is due to basal metabolic costs. At higher particle-attached bacterial abundances, more exoenzyme is produced and the cost of exoenzymes is distributed among a larger group of particle-attached bacteria. The greater concentration of exoenzymes generates enough hydrolysate for particle-attached bacterial uptake to be closer to maximum rates. Once exoenzymes generate enough hydrolysate for particle-attached bacterial uptake to reach maximum rates, producing additional exoenzymes adds energetic cost without benefit. Thus, $\epsilon = 0.05$ h^{-1} results in lower particle-attached bacterial production than $\epsilon = 0.01$ to 0.03 h^{-1} (Fig. 2).

b. Optimal exoenzyme production rate

The threshold particle-attached bacterial abundance above which exoenzyme production is a viable option (i.e., particle-attached bacterial production is greater than 0) is revealed by plotting the exoenzyme production rate producing the highest bacterial abundance in Figure 2 against bacterial abundance (Fig. 3). *Interior* and *Interception* scenarios have a similar shape that increases from the zero growth thresholds to a maximum value (Fig. 3). The threshold particle-attached bacterial abundance for viable exoenzyme production in the *Interception* scenario is 7.8×10^6 bacteria particle^{-1}, and in the *Interior* scenario is 9.3×10^6 bacteria particle^{-1}. In contrast to the *Interior* and *Interception* scenarios, optimal exoenzyme production in the *Retention* scenario increases from a threshold to a maximum value and then decreases again to a constant value (Fig. 3). The threshold particle-attached bacterial abundance for the *Retention* scenario is the lowest, 5.5×10^6 bacteria particle^{-1}, equivalent to 22% bacterial coverage of the particle surface area. It is energetically "optimal" for

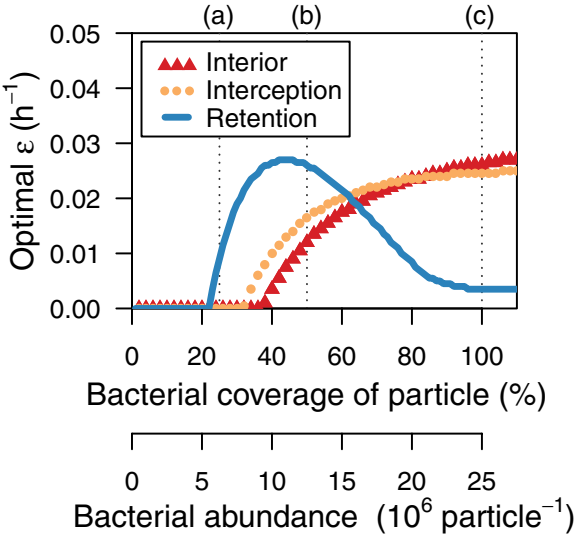

Figure 3. Emergent patterns of optimal exoenzyme production rates, ε, are related to particle-attached bacterial abundance. Optimal exoenzyme production rates are the exoenzyme production rates that result in the greatest particle-attached bacterial production. Diagrams of particle-attached bacterial distribution on particles associated with *Interior*, *Interception*, and *Retention* are in Figure 2. (a), (b), and (c) indicate exoenzyme production when particle-attached bacterial abundances are 6.3×10^6 (a), 1.3×10^7 (b), and 2.5×10^7 (c), which are equivalent to 25%, 50%, and 100% bacterial coverage of particles.

particle-attached bacteria to produce lower quantities of exoenzyme at high particle-attached bacterial abundances in the *Retention* scenario because diffusive losses of exoenzyme and hydrolysate from the particle are reduced. In other words, particle-attached bacteria continue to take up hydrolysate at maximum rates because the concentrations of exoenzyme and hydrolysate in the particle remain high despite lower new exoenzyme production. The optimal ϵ results shown in Figure 3 are incorporated into the model to determine the effect of exoenzyme production on carbon flux in the water column; more details are in given the Appendix (equation A19; Tables A2, A3).

c. Carbon flux profiles

The model demonstrates that colonization of particles by bacteria in the euphotic zone is a primary determinant of carbon flux attenuation within the mesopelagic zone (Fig. 4). This is because the concentration of free-living bacteria decreases exponentially with depth (Li and Harrison 2001), which causes slow particle colonization rates within the mesopelagic zone in the model (Kiørboe et al. 2002). Very little particulate carbon is decomposed and remineralized by particle-attached bacteria when abundance is 6.3×10^6 bacteria particle^{-1}

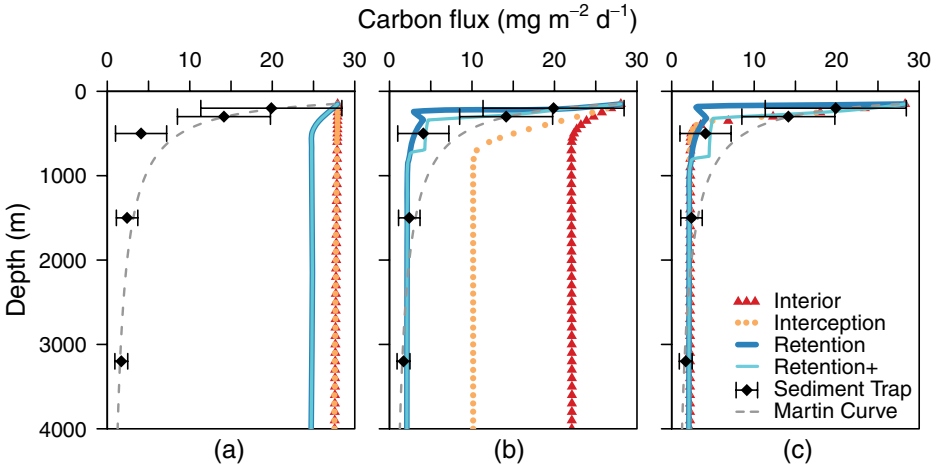

Figure 4. Carbon flux in the Sargasso Sea, North Atlantic Ocean. The model is forced with particles sinking from the euphotic zone, which have particle-attached bacterial abundances of 6.3×10^6 (a), 1.3×10^7 (b), and 2.5×10^7 (c), which are equivalent to 25%, 50%, and 100% bacterial coverage of particles. *Interior*, *Interception*, and *Retention* profiles are model results for the flux of particulate carbon, which includes both particulate carbon and particle-attached bacteria. *Retention+* is the sum of particulate carbon and the solute carbon for the *Retention* scenario. Solute carbon is the flux of hydrolysate and exoenzyme retained in the particle. Sediment trap data are mean $\pm$ standard deviation. The power law fit to the sediment trap data resulted in an exponent, $b = 0.94$ (Martin et al. 1987).

(25% coverage) on particles fluxing from the euphotic zone (Fig. 4a). At a higher abundance of 1.3×10^7 bacteria particle^{-1} (50% coverage), decomposition and remineralization increase, and there are large variations among the scenarios (Fig. 4b). Carbon flux in the *Retention* scenario is much more similar to sediment trap measurements than carbon flux in the *Interior* and *Interception* scenarios (Fig. 4b). The variation among the scenarios is greatly reduced once abundances reach 2.5×10^7 bacteria particle^{-1} (100% coverage), and particle fluxes in all the scenarios are similar to sediment trap measurements (Fig. 4c).

The remineralization e-folding depth, the depth at which 63% of carbon is removed from particles (e.g., Kwon, Primeau, and Sarmiento 2009) is used as a benchmark to compare the carbon flux dynamics of the model results in Figure 4(c) (i.e., complete initial coverage) with a power law fit to the sediment trap data (Martin et al. 1987). The remineralization e-folding depth for the power law is 435 m. The remineralization e-folding depths for the *Interior*, *Interception*, and *Retention* scenarios in Figure 4(c) are shallower (316, 304, and 167 m, respectively) for particulate carbon, which is the combined flux of particulate organic matter and particle-attached bacteria. In the microbial remineralization model, there is an additional form of carbon, solute carbon, the combination of hydrolysate and exoenzymes, which is transported within the particle. The e-folding depth for the combined flux of particulate and solute carbon in the *Retention* scenario, referred to as *Retention+* in Figure 4(c), is 291 m.

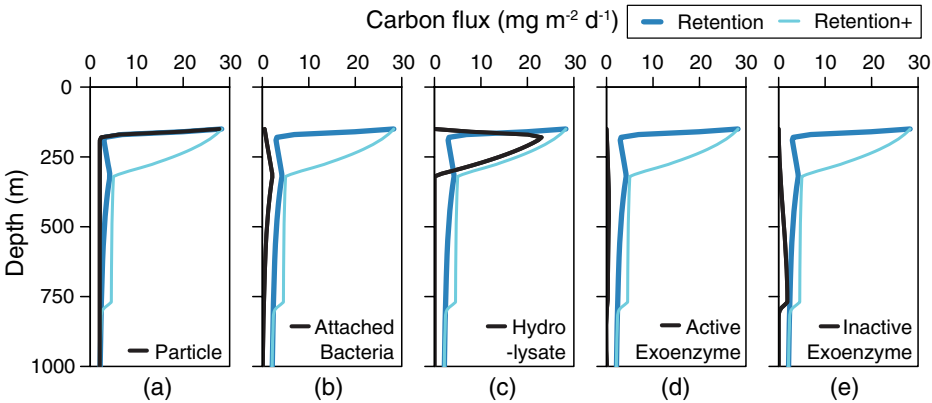

Figure 5. Carbon flux of each variable in the *Retention* scenario when particle-attached bacterial abundance is 2.5×10^7 (100% coverage) on particles fluxing from the euphotic zone. Carbon fluxes for *Retention* and *Retention+* from Figure 4(c) are plotted in all the panels. The *Retention* profile is the flux of particulate carbon, the sum of panels (a) and (b). *Retention+* is the combination of particulate carbon and solute carbon, the sum of panels (a), (b), (c), (d), and (e). The depth range plotted is from 0 to 1,000 m to expand the upper water column. The carbon flux of individual variables changes with depth often with sharp transitions as the carbon in the particles is decomposed and utilized by particle-attached bacteria.

The flux of solute carbon in the *Interior* and *Interception* scenarios is very small and does not alter the pattern of carbon flux.

There are abrupt transitions in the carbon flux profiles for the *Retention* scenario (Fig. 4b and c). The transitions in *Retention* are related to the following processes in the model: Particulate carbon is rapidly decomposed to hydrolysate, which is retained in the particle by the particle-attached bacteria but is no longer in particulate form, causing the rapid decrease in "particulate" carbon flux between 150 and 200 m depth (Fig. 5a and c). As these processes are occurring, the size and sinking speed of the particles are maintained by calcium carbonate, opal, and lithogenic material. The particle-attached bacteria use the retained hydrolysate to grow quickly producing the increase in "particulate" carbon flux from 200 to 320 m depth (Fig. 5b). However, most of the hydrolysate is used for respiration, so the increase in "particulate" carbon flux is tempered relative to the initial decrease in "particulate" carbon flux. The pool of hydrolysate in the particles is limited by the initial amount of carbon in the particles when they sink into the mesopelagic zone. Therefore, the hydrolysate is eventually used up causing the gradual decrease in "particulate" carbon flux below 320 m as exoenzyme production, detachment, and mortality processes deplete the concentration of particle-attached bacteria (Fig. 5b).

Retention+ includes hydrolysate, active exoenzyme, and inactive exoenzyme as well as particulate material and particle-attached bacteria. The combination of these fluxes also results in abrupt transitions in the carbon flux profile (Fig. 4b and c). Carbon flux decreases

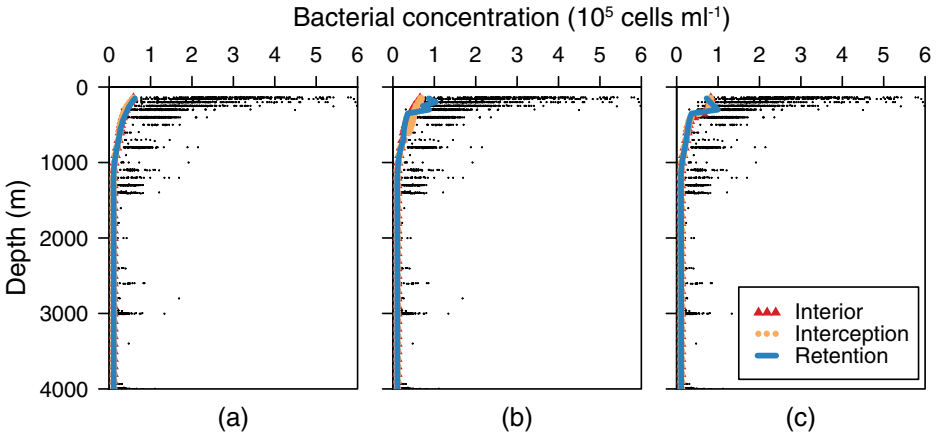

Figure 6. The effects of *Interior*, *Interception*, and *Retention* scenarios on free-living bacterial concentrations in the water column for particle-attached bacterial abundances of 6.3×10^6 (a), 1.3×10^7 (b), and 2.5×10^7 (c) on particles fluxing from the euphotic zone. The black dots are measurements of picoheterotroph concentrations from the BATS station. The higher bacterial abundances, 1.3×10^7 and 2.5×10^7, on the particles fluxing from the euphotic zone increased the concentrations of free-living bacteria between 150 and 400 m depth.

between 150 and 320 m. The decrease is rapid but slower than the decrease for "particulate" carbon flux because all forms of organic carbon are included in the flux and the decrease is mainly due to particle-attached bacterial respiration. Once the hydrolysate is consumed, particle-attached bacteria and exoenzymes continue to sink to deeper depths (Fig. 5). The exoenzymes, both active and inactive, are released from the particles at ~690 m in Figure 4(b) and ~770 m in Figure 4(c) causing the rapid drop in carbon flux. The exoenzymes are released because the particle-attached bacterial biomass shrinks due to exoenzyme production, detachment, and mortality and no longer physically retains the exoenzymes in the particles. In the model, the effect of biofilms is directly related to particle-attached bacterial biomass, so depletion in particle-attached bacterial biomass also "degrades" the biofilms in the particle.

d. Free-living bacterial concentration

Free-living bacterial concentration increases between 150 m and 400 m when particle-attached bacterial abundance on particles fluxing from the euphotic zone increases from 6.3×10^6 to 2.5×10^7 (Fig. 6). This increase in free-living bacterial concentration was similar among the *Interior*, *Interception*, and *Retention* scenarios. However, there are abrupt transitions in the vertical profile of free-living bacterial concentration in the *Retention* scenario (Fig. 6b and c). We also compared free-living bacterial concentrations from the microbial remineralization model with data from the BATS station and found that modeled

free-living bacterial concentrations are at the lower threshold of picoheterotroph concentrations from BATS (Fig. 6). Reasons for the abrupt transitions and the lower free-living bacterial concentrations in the model results are discussed in the next section.

4. Discussion

a. Group behavior of particle-attached bacteria

There is some debate as to the reason that bacteria use signaling molecules—whether it is to assess local bacterial population density or the diffusion environment (West et al. 2012). Our results show that on sinking particles in the ocean, diffusive processes provide an impetus for coordinated group behavior among particle-attached bacteria as was hypothesized by Vetter et al. (1998). The increase in particle-attached bacterial uptake efficiency when particle-attached bacterial abundances are high allows more of the hydrolysate to be utilized by particle-attached bacteria before it diffuses away, thereby increasing overall particle-attached bacterial productivity (Fig. 2). Furthermore, the cost of producing exoenzymes is shared among particle-attached bacteria. There is an abundance threshold at which producing exoenzymes becomes energetically beneficial for the group as a whole (Fig. 3), so using signaling molecules to both coordinate a type of exoenzyme and the timing of exoenzyme production is an energetically effective strategy. Thus, the model provides a theoretical justification for the previous lab and field observations that groups of particle-attached bacteria use quorum sensing to coordinate production of exoenzymes on sinking particles.

The scenarios depicted in Figure 2 are not necessarily alternatives but may actually be a succession of conditions that occur on particles as they sink. Jing et al. (2012) observed community structure changes on copepod fecal pellets, one type of marine particle, and found that the bacterial communities on fecal pellets and in the dissolved environment are initially different, but over time, bacterial communities on fecal pellets become more similar to bacterial communities in the dissolved environment. The initial bacterial community may be in fecal pellets as they are egested either from incompletely digested food or the gut (Nagasawa and Nemoto 1988) (Fig. 2a). As free-living bacteria encounter particles, they colonize the surface of the particle as a first step (e.g., Honjo and Roman 1978; Jacobsen and Azam 1984) (Fig. 2b). Then particle-attached bacterial cells cooperatively produce exoenzymes and biofilms (Drescher et al. 2014). The decrease in advective and diffusive losses in biofilms serves to greatly increase particle-attached bacterial production (Fig. 2c). The much higher particle-attached bacterial production calculated for the *Retention* scenario in Figure 2(c) would likely offset the additional energetic cost associated with producing biofilms.

The *Retention* mechanism in the microbial remineralization model is assumed to be solely dependent on particle-attached bacteria. However, the shapes and compositions of particles may also slow transfer rates of exoenzymes and hydrolysates from particles. The shape of the particles was assumed to be spherical in the microbial remineralization model, but

natural particles are amorphous with complex internal structures (Alldredge and Gotschalk 1988). The internal structures, particularly if mucus is present, may hinder transfer rates of exoenzymes and hydrolysates from the particle (Hannides, Dunn, and Aller 2005). By altering transfer rates, the physical structure of the particles may affect biological interactions, in particular the balance between cooperation and competition among attached bacteria. Attached bacteria that do not produce exoenzymes outgrow attached bacteria that produce exoenzymes when solubilized nutrients are available to both producers and nonproducers (Drescher et al. 2014). Under these conditions, there would not appear to be a selective advantage to cooperate to produce exoenzymes. Flow helps select for cooperation to produce exoenzymes by constricting the area over which solubilized nutrients are available closer to the origins of exoenzyme production within biofilms, which benefits the exoenzyme producers (Drescher et al. 2014). Therefore, particle structures that greatly decrease transfer rates of exoenzymes and hydrolysate from particles may not necessarily promote selection for group behavior among bacteria to produce exoenzymes. These would be interesting points to explore in models that include more complex characterizations of particles and bacteria.

b. Biogeochemical implications of group behavior

Bacterial abundance on particles has consequences for remineralization length scales (Fig. 4). The *Interior* and *Interception* scenarios require higher threshold particle-attached bacterial abundances for the inception of exoenzyme production than the *Retention* scenario (Fig. 3). There is no attenuation of particle flux in the *Interior* and *Interception* scenarios in Figure 4(a) because the particle-attached bacterial abundances fluxing from the euphotic zone are below the threshold for the inception of exoenzyme production (dotted line (a) in Fig. 3). Once particle-attached bacterial abundances exceed the thresholds (dotted lines (b) and (c) in Fig. 3), particle flux attenuates (Fig. 4b and c). In a laboratory study, Jacobsen and Azam (1984) observed maximum particle-attached bacterial abundance equivalent to 27% coverage of a particle and slow decomposition rates, conditions most similar to Figure 4(a). This result emphasizes the importance of a *Retention* mechanism for particle decomposition when bacterial abundances per particle are low.

Conditions in the natural environment (e.g., advection, particle sinking, and chemoattraction) likely increase the number of bacteria contacting a particle (Jacobsen and Azam 1984; Kiørboe et al. 2002; Stocker and Seymour 2012). The results in Figure 4 suggest that variation in bacterial colonization rates due to these environmental factors may influence the length scales of remineralization and the dynamics of the mesopelagic food web by enhancing the ability of bacteria to utilize carbon in particles. If colonization is rapid, particle-attached bacteria working in groups can solubilize and consume large, fast-sinking particles that typically have been assumed to be consumed as food or broken up by "sloppy feeding" by large zooplankton (Giering et al. 2014). Exoenzyme activity has the potential to alter competition between bacteria and zooplankton for particulate organic carbon

by rapidly solubilizing particles into molecules too small for larger zooplankton to ingest. Also, enhanced bacterial production resulting from exoenzyme activity may provide an important prey for microzooplankton (Kiørboe et al. 2003). There is great need for more observations of bacterial abundances per particle to help determine the regional importance of particle-attached bacteria in the global ocean.

Climate models often use parameterizations similar to the power law, the "Martin curve" in Figure 4, to represent the flux of particulate carbon. The microbial remineralization model results suggest that the "Martin curve" may be insufficient for quantifying carbon remineralization in the mesopelagic zone at BATS. The power law has shallower remineralization than the microbial remineralization model does when bacterial abundances on particles are low and deeper remineralization than the microbial remineralization model does when bacterial abundances on particles are high (Fig. 4). In Figure 4(c), which shows the results when the modeled particles have the highest bacterial abundances, the average remineralization e-folding depth across all the bacterial arrangements is 270 m, which is 165 m shallower than the remineralization e-folding depth of 435 m for the power law. Notably, the modeled particle fluxes in Figure 4(c) are more similar to sediment trap data, especially at 500 m, than the power law fit to the data. The sensitivity of atmospheric CO_2 to a shift in remineralization e-folding depth from 400 m to 250 m is 10–55 ppm, which could be the impact on atmospheric CO_2 if the remineralization e-folding depth is being underestimated globally (Kwon, Primeau, and Sarmiento 2009).

c. Solute carbon

Solutes are an additional complication in the *Retention* scenario. Solutes not immediately remineralized in the *Retention* scenario are transported within the particle. Accounting for the contribution of solute carbon to the carbon flux deepened the remineralization e-folding depth for the *Retention* scenario (*Retention*+, Fig. 4b and c). Supernatant from poisoned sediment traps deployed in the mesopelagic zone was found to have higher concentrations of dissolved nutrients including organic carbon than deeper traps (Antia 2005). The existence of organic carbon in supernatant is potentially circumstantial evidence that a retention mechanism is employed by bacteria on particles, and dissolved nutrients are transported into sediment traps inside particles. Thus, the *Retention* scenario, which has already been linked previously to enhanced bacterial production and relatively lower bacterial abundance thresholds for viable exoenzyme production and associated particle solubilization, is also consistent with biogeochemical findings from sediment traps.

Particles are a source of dissolved organic carbon that can be consumed by free-living bacteria in the *Retention* scenario in agreement with the existing paradigm (Smith et al. 1992), except in the extreme case of 100% retention efficiency of biofilms. The extreme case is modeled to provide an outer boundary of potential conditions. A scenario more representative of natural environments is that the transfer of solute carbon out of the particles to the dissolved environment is reduced by biofilms but is never 100% efficient.

Another feature of the *Retention* scenario is that solute carbon trapped by the biofilms but not consumed by particle-attached bacteria can be released in a pulse to the dissolved environment if/when the biofilms degrade. In the model results, pulses of solute carbon into the dissolved environment occur when there is the rapid drop in *Retention*+ carbon flux at ∼690 m in Figure 4(b) and ∼770 m in Figure 4(c). Such pulses of solute carbon may lead to an observable signature of localized concentrations of dissolved organic carbon. Hydrolysate and exoenzymes are a small fraction of dissolved organic carbon in the ocean, so unfortunately, it is not possible to analyze existing measurements of bulk dissolved organic carbon to determine if such signatures of solute carbon occur (Hansell 2013). As dissolved organic carbon becomes more fully characterized (e.g., Aluwihare et al. 2005; Orellana and Hansell 2012), it may be possible to identify the solute carbon fraction of dissolved organic carbon. Patterns of solute carbon in the water column can then be related to dissolved exoenzyme activities (Baltar et al. 2010).

d. Free-living bacterial concentration

The group behavior of attached bacteria on particles influences free-living bacterial concentrations in the microbial remineralization model results. There is no degradation of particulate carbon for the *Interior* and *Interception* scenarios and little degradation of particulate carbon for the *Retention* scenario when the abundance of particle-attached bacteria fluxing from the euphotic zone is 6.3×10^6, 25% coverage of the particle (Fig. 4a). Therefore, there is little to no hydrolysate diffusing from the particles, no detachment of particle-attached bacteria, and little to no exoenzymes diffusing from the particles. For growth, free-living bacteria take up dissolved hydrolysate that forms when semilabile dissolved organic carbon decays. Consequently, the profiles of the vertical distribution of free-living bacterial concentration in all the scenarios, *Interior*, *Interception*, and *Retention*, in Figure 6a are similar to the profile of the vertical distribution of semilabile organic carbon (DOC_s in Fig. A1). Degradation of particulate carbon occurred when particle-attached bacterial concentrations fluxing from the euphotic zone were 1.3×10^7, 50% coverage of the particle, and 2.5×10^7, 100% coverage of the particle (Fig. 4b and c). The degradation of the particles impacted the free-living bacteria. Free-living bacterial concentrations between 150 and 400 m depth in Figure 6(b) and (c) were higher than the free-living bacterial concentrations at the same depths in Figure 6(a).

There are abrupt transitions in the vertical profile of the free-living bacterial concentration in the *Retention* scenario because the patterns of exchange between the particle and the dissolved environments are altered (Fig. 6b and c). Particle-attached bacteria impede the transfer of hydrolysate from the particle to the dissolved environment causing a reduction in the growth of free-living bacteria which decreases free-living bacterial concentration. The subsequent rapid growth of particle-attached bacteria occurs because there is more hydrolysate in the particles resulting in an increase in the detachment rate which increases free-living bacterial concentration. Abrupt transitions occur because shifts to the domination

of one or the other of these mechanisms occur at different depths in the water column (*Retention*, Fig. 6b and c). In contrast, there are more gradual shifts in hydrolysate transfer out of particles and bacterial detachment from particles in the *Interior* and *Interception* scenarios (Fig. 6b and c).

The vertical profiles of free-living bacterial concentrations in the model results were similar to the vertical profiles of picoheterotroph concentrations from BATS. Both profiles included a decrease in concentration between 150 and 1,000 m depth and little change in concentration between 1,000 and 4,000 m depth (Fig. 6). However, free-living bacterial concentrations from the model were at the lower edge of the picoheterotroph concentrations from BATS (Fig. 6). Picoheterotroph is a term for the combination of heterotrophic bacteria and archaea, which are not differentiated in the BATS data (Buitenhuis et al. 2012). In the deep Atlantic, bacteria have been measured to be approximately 30% of the picoplankton (Herndl et al. 2005; Teira et al. 2006). The model is based on studies of heterotrophic bacteria, so the BATS concentrations may be higher because they also include archaea. The parameterizations of the model might also be causing the discrepancy between the model results and the BATS data. Free-living bacteria are influenced by physical, chemical, and biological factors in the dissolved environment that are not presently included in the model (e.g., Carlson, Ducklow, and Michaels 1994), and inclusion of these additional factors might increase free-living bacterial concentrations.

e. Conclusions

This version of the microbial remineralization model is the first step toward assembling complex biological processes driving the solubilization of sinking particles into a single predictive framework. The model has already generated some intriguing hypotheses including the following: (1) Clogging that results in retention of exoenzymes and hydrolysate in particles increases particle-attached bacterial production. (2) Particle-attached bacteria reduce exoenzyme production at high abundances when diffusive losses are minimized via a mechanism such as biofilms. (3) Solubilized nutrients are transported to deeper depths in sinking particles that are clogged. (4) Particle-attached bacterial abundance per particle at the base of the euphotic zone influences remineralization depths. Additional processes to be explored in the microbial remineralization model include particle size, particle sinking speed, and exoenzyme activity rates. The microbial remineralization model will also be expanded to include more ecosystem components that interact with particles such as zooplankton. Field and laboratory studies that both improve parameterizations in the model and serve as verification for model results are essential for the robust mechanistic characterization and calibration of the microbial remineralization model.

The emergence of a relationship between exoenzyme production and particle-attached bacterial abundance in the model suggests that quorum sensing is an effective strategy for exoenzyme production on particles. Particle-attached bacteria coordinating exoenzyme production using quorum sensing have the potential to increase particle-attached bacterial

production on particles and shoal particulate carbon remineralization. *Interior, Interception*, and *Retention* conditions are also important in the resulting efficiency of both quorum sensing and overall remineralization. Future observations should quantify regional and temporal variability in the abundances of bacteria per particle and determine whether exoenzymes and hydrolysate are retained in particles in the mesopelagic zone. These efforts will help improve projections of the impact of bacterial group behavior on ocean carbon cycling and global climate.

Acknowledgments. KAS was supported by the NOAA Cooperative Institute for Climate Science (NA08OAR4320752) and the Carbon Mitigation Initiative, which is sponsored by BP. Data from the BATS was essential for the development of the model. Discussions with D. Bianchi, A. Gnanadesikan, N. Wingreen, K. Drescher, and P. Jumars greatly benefitted the study. Comments by R. Aller, P. Franks, and anonymous reviewers improved this manuscript.

APPENDIX

a. Microbial remineralization model equations

The microbial remineralization model is based on a one-dimensional Eulerian framework. The depth range of the model is from the base of the euphotic zone to the ocean bottom in 10 m depth intervals. The time step is 30 s. Carbon in mg m^{-3} seawater is traced through nine biological compartments including particulate organic carbon (POM), particle-attached bacteria (PB), free-living bacteria (DB), active exoenzyme in the particle (EP), inactive exoenzyme in the particle (XP), hydrolysate in the particle (HP), hydrolysate in the dissolved environment (HD), active exoenzyme in the dissolved environment (ED), and inactive exoenzyme in the dissolved environment (XD) (Fig. 1). Remineralized inorganic carbon (CO_2) is not modeled explicitly. We assume that CO_2 produced by bacterial respiration is eventually transported by mixing and large-scale circulation to the ocean surface where phytoplankton take it up and convert it to organic carbon during photosynthesis. Some of the organic carbon then becomes new sinking particles. Rates of change in concentration are calculated using the following set of equations:

$$\frac{d\mathrm{POM}}{dt} = m_{\mathrm{PB}}\mathrm{PB}^{2} - \gamma\mathrm{EP} + w\frac{d\mathrm{POM}}{dz} \tag{A1}$$

$$\frac{d\mathrm{PB}}{dt} = \mu_{\mathrm{PB}}\mathrm{PB} + \beta\mathrm{DB} - \delta\mathrm{PB} - m_{\mathrm{PB}}\mathrm{PB}^{2} + w\frac{d\mathrm{PB}}{dz} \tag{A2}$$

$$\frac{d\mathrm{DB}}{dt} = \mu_{\mathrm{DB}}\mathrm{DB} + \delta\mathrm{PB} - \beta\mathrm{DB} - m_{\mathrm{DB}}\mathrm{DB}^{2} \tag{A3}$$

$$\frac{d\mathrm{EP}}{dt} = \epsilon\mathrm{PB} - \Theta q_{\mathrm{EP}}(\mathrm{EP}_{p} - \mathrm{ED}) - m_{\mathrm{E}}\mathrm{EP} + w\frac{d\mathrm{EP}}{dz} \tag{A4}$$

$$\frac{d\mathrm{XP}}{dt} = m_{\mathrm{E}}\mathrm{EP} - \Theta q_{\mathrm{XP}}(\mathrm{XP}_{p} - \mathrm{XD}) - \kappa\mathrm{XP} + w\frac{d\mathrm{XP}}{dz} \tag{A5}$$

$$\frac{d\mathrm{HP}}{dt} = \gamma \mathrm{EP} + \kappa \mathrm{XP} - \Theta q_{\mathrm{HP}}(\mathrm{HP}_p - \mathrm{HD}) - v_{\mathrm{PB}}\mathrm{PB} + w\frac{d\mathrm{HP}}{dz} \quad \text{(A6)}$$

$$\frac{d\mathrm{HD}}{dt} = \kappa \mathrm{DOC}_s + \kappa \mathrm{XD} + \Theta q_{\mathrm{HP}}(\mathrm{HP}_p - \mathrm{HD}) + m_{\mathrm{DB}}\mathrm{DB}^2 - v_{\mathrm{DB}}\mathrm{DB} \quad \text{(A7)}$$

$$\frac{d\mathrm{ED}}{dt} = \Theta q_{\mathrm{EP}}(\mathrm{EP}_p - \mathrm{ED}) - m_{\mathrm{E}}\mathrm{ED} \quad \text{(A8)}$$

$$\frac{d\mathrm{XD}}{dt} = m_{\mathrm{E}}\mathrm{ED} + \Theta q_{\mathrm{XP}}(\mathrm{XP}_p - \mathrm{XD}) - \kappa \mathrm{XD} \quad \text{(A9)}$$

Symbols from these equations are described in the following sections. The model parameters are in Tables A1, A2, and A3. The model is forced with particle flux at the base of the euphotic zone and POM has a sinking rate, w. PB, EP, XP, and HP, which are associated with the particles, also have a sinking rate, w. Sinking components experience depth-related changes in environmental variables. Vertical profiles of temperature (T), salinity (S), density (ρ) are used to calculate dynamic viscosity, kinematic viscosity, and temperature-dependent biological rates (Fig. A1).

In the microbial remineralization model, HD, ED, and XD are supplied to the dissolved environment through mass transfer from the sinking POM (Fig. 1), but this is only a small fraction of the dissolved organic carbon (DOC) in the ocean. Additional DOC is supplied to deeper depths through deep mixing and large-scale ocean circulation (Carlson et al. 1994; Hansell and Carlson 2001), physical processes not included in this model. Most DOC is refractory, which breaks down over century timescales and so does not significantly contribute to free-living bacterial food sources, HD, on a daily basis (Hansell 2013).

However, semilabile DOC, DOC_s, decays on a much faster time scale $\leq$ 5 years, and needs to be considered as an HD source for free-living bacteria in the mesopelagic zone (Abell, Emerson, and Renaud 2000; Hansell 2013). External nutrient sources are supplied to HD using decay, κ, from a vertical profile of DOC_s (Fig. A1).

The model uses parameters and data (Fig. A1, Table A1) from the BATS study (31°40'N, 60°10'W), which is located in the western North Atlantic subtropical gyre. BATS was selected because the data include 20+ years of biological and physical data as well as numerous published studies on the biological and biogeochemical processes. BATS data variables are collected at least once a month and more frequently during the spring bloom period (Steinberg et al. 2001). We use the following BATS data: temperature, salinity, DOC, and particle fluxes at 150, 200, and 300 m. Average particle flux, 27.8 mg m^{-2} d^{-1}, at 150 m is used for forcing in the model. Particle-attached bacteria, hydrolysate, and exoenzymes have not been quantified at BATS. In the model, we assume that particles fluxing in at the upper vertical boundary have already been colonized by bacteria but exoenzymes and hydrolysate have not yet been produced. The model simulates carbon flux in the water column, which can be compared to data from deeper sediment traps. In addition to the BATS sediment traps at 200 and 300 m, the OFP has sediment traps permanently moored at 500, 1,500, and 3,200 m depths to measure particle fluxes near the BATS site

Table A1. Model parameters for one-dimensional vertical model of sinking particles. In the descriptions: C is carbon, B is bacteria, E is exoenzyme, and H is hydrolysate. The characteristics of the model exoenzyme are based on leucine aminopeptidase which catalyzes the hydrolysis of the amino acid leucine to hydrolysate.

Symbol	Description	Value	Units	Reference
r	Particle radius	1	mm	
w	Particle sinking speed	48	m d^{-1}	Alldredge and Gotschalk (1988)
$R_{C:W_{\mathrm{dry}}}$	C per particle dry weight	0.12	mg C (mg W_{dry})$^{-1}$	Iversen et al. (2010)
$R_{C:B}$	C per bacterium	5	fg C (cell)$^{-1}$	Gundersen et al. (2002)
B_{GEmax}	Max B growth efficiency	0.4		del Giorgio and Cole (2000)
Υ	B basal metabolism	0.002	h^{-1}	
k_{HD}	Uptake half-saturation	30	mg C m^{-3}	Christian and Anderson (2002)
k_{HP}	Uptake half-saturation	200	mg C m^{-3}	Christian and Anderson (2002)
v_{max}	Max uptake	0.25*	h^{-1}	μ_{max}/B_{GEmax}
γ_{max}	Max E activity	118*	h^{-1}	Steen and Arnosti (2011)
$t_{1/2}$	E half-life	30*	h	Steen and Arnosti (2011)
u	DB swimming speed	0.09	m h^{-1}	Kiørboe et al. (2002)
τ	DB run length	0.002	h	Kiørboe et al. (2002)
α	The cos($\angle$) between DB runs	−0.67		Kiørboe et al. (2002)
m_{DB}	Mortality DB	0.02	h^{-1} (mg C)$^{-1}$ m^3	
m_{PB}	Mortality PB	0.04	h^{-1} (mg C)$^{-1}$ m^3	
l_B	Length B	1	μm	Kirchman (2012)
d_B	Diameter B	0.5	μm	Kirchman (2012)
r_H	Radius of H molecule	0.15	nm	Rawn (1989)
r_E	Radius of E molecule	4.9	nm	Burley et al. (1990)
$R_{M:C}$	Ratio of total mass to C mass of leucine	1.8		
ρ_M	Leucine density	1.29	g cm^{-3}	Haynes (2012)
$f_{\mathrm{CaCO_3}}$	$CaCO_3$ fraction	0.075	mg C (mg $CaCO_3$)$^{-1}$	Klaas and Archer (2002)
f_{opal}	Opal fraction	0.029	mg C (mg opal)$^{-1}$	Klaas and Archer (2002)
f_{lith}	Lithogenic fraction	0.052	mg C (mg lith.)$^{-1}$	Klaas and Archer (2002)
$\Phi_{\mathrm{CaCO_3}}$	Flux $CaCO_3$	21	mg m^{-2} d^{-1}	Conte, Ralph, and Ross (2001)
Φ_{opal}	Flux opal	4.34	mg m^{-2} d^{-1}	Conte, Ralph, and Ross (2001)
Φ_{lith}	Flux lithogenic	6.77	mg m^{-2} d^{-1}	Conte, Ralph, and Ross (2001)
DOC_r	Deep refractory DOC	43.6	mmol m^{-3}	Hansell and Carlson (2001)
t_{DOC}	DOC turnover time	5	years	Abell, Emerson, and Renaud (2000)
k_b	Boltzman constant	1.38×10^{-23}	kg m^2 s^{-1} K^{-1}	
ν	Kinematic viscosity	Variable**	m^2 s^{-1}	Jumars et al. (1993)
η	Dynamic viscosity	Variable**	kg m^{-1} s^{-1}	Jumars et al. (1993)
Q_{10}	Temperature scaling	2		Dell, Pawar, and Savage (2011)

*Temperature-dependent value at 20°C.

**Dependent on temperature, salinity and density; see the appendix of Jumars et al. (1993) for equations.

(Conte, Ralph, and Ross 2001). The vertical profiles of temperature, salinity, density, and DOC_s used in the model are in Figure A1. The temperature, salinity, and density data are long-term averages from conductivity, temperature, depth sensor measurements collected monthly at BATS between 1988 and 2011. The DOC_s profile is a long-term average of

Table A2. Parameters to calculate the optimal exoenzyme production rate, optimal ϵ (h^{-1}), for the *Interior* and *Interception* bacterial arrangement scenarios using equation (A19) (cf. Fig. 3). The values for bacterial biomass (mg particle^{-1}) are converted to bacterial abundance (cells particle^{-1}) using the fg carbon per bacterium conversion factor $R_{C:B}$ in Table A1.

Symbol	Description	Value	Units
Interior			
θ_ϵ	Exoenzyme production threshold	9.3×10^6	cells particle^{-1}
ϵ_{max}	Maximum exoenzyme production	0.027	h^{-1}
k_ϵ	Half production constant	1.3×10^7	cells particle^{-1}
x	Exponent	1.42	
Interception			
θ_ϵ	Exoenzyme production threshold	7.8×10^6	cells particle^{-1}
ϵ_{max}	Maximum exoenzyme production	0.025	h^{-1}
k_ϵ	Half production constant	1.1×10^7	cells particle^{-1}
x	Exponent	1.44	

depths with >100 total data points (1990–2010) from bottles that are smoothed using least squares in a local polynomial regression fit (loess). Smoothing decreases the sharp transitions between data from unevenly spaced depths preventing artificial features in the model results.

Parameterizations were adjusted to explore the effects of bacterial arrangement linked to nutrient flux conditions on bacterial production. The following arrangement scenarios were used: (1) *Interior*, in which bacteria are in the particle and take up hydrolysate in the particle; (2) *Interception*, in which bacteria intercept hydrolysate as it leaves the particle; and (3) *Retention*, in which bacteria take up or retain hydrolysate in particles. In the *Retention* scenario, active and inactive exoenzyme are retained in addition to the hydrolysate. The terms *Interior*, *Interception*, and *Retention* will be used in the following text to identify changes in the model parameterizations for each of the scenarios.

b. Particle characteristics

POM is traced as the concentration of particulate organic matter per volume seawater in the ecosystem model framework (equations A1–A9). To realistically model biological processes on the particles, it is necessary to specify particle characteristics including number, size, and composition. Particle-based processes are incorporated by using dimensionless ratios for scaling or by multiplying an individual particle concentration by the total number of particles per volume of seawater. Some simplifications were made to allow for initial exploration of bacterial behavior on sinking particles. The particles in the model are spherical in shape, and this study focused on a single size, a radius of 1 mm. Another characteristic of the model is that ballast and other inedible materials prevent sinking particles from disappearing or changing size. The microbial remineralization model can eventually be

Table A3. Lookup table to determine the optimal exoenzyme production rate, optimal ϵ, for the *Retention* scenario (cf. Fig. 3). ϵ (h^{-1}) is determined using bacterial abundance (cells $particle^{-1}$). The values for bacterial biomass (mg $particle^{-1}$) are converted to bacterial abundance (cells $particle^{-1}$) using the fg carbon per bacterium conversion factor $R_{C:B}$ in Table A1. The particle is $\geq$100% covered by particle-attached bacteria when particle-attached bacterial abundance $\geq 2.51 \times 10^7$, the highest abundance in the table. ϵ is produced at a constant rate of 0.0035 h^{-1} above this threshold.

Abundance	ϵ	Abundance	ϵ	Abundance	ϵ	Abundance	ϵ
2.51×10^5	0	6.53×10^6	0.0115	1.28×10^7	0.0255	1.91×10^7	0.011
5.02×10^5	0	6.78×10^6	0.0135	1.31×10^7	0.0255	1.93×10^7	0.01
7.54×10^5	0	7.03×10^6	0.0155	1.33×10^7	0.025	1.96×10^7	0.0095
1.00×10^6	0	7.28×10^6	0.0175	1.36×10^7	0.0245	1.98×10^7	0.009
1.26×10^6	0	7.54×10^6	0.019	1.38×10^7	0.024	2.01×10^7	0.0085
1.51×10^6	0	7.79×10^6	0.02	1.41×10^7	0.0235	2.03×10^7	0.0075
1.76×10^6	0	8.04×10^6	0.0215	1.43×10^7	0.023	2.06×10^7	0.007
2.01×10^6	0	8.29×10^6	0.0225	1.46×10^7	0.0225	2.08×10^7	0.0065
2.26×10^6	0	8.54×10^6	0.0235	1.48×10^7	0.022	2.11×10^7	0.006
2.51×10^6	0	8.79×10^6	0.024	1.51×10^7	0.0215	2.14×10^7	0.0055
2.76×10^6	0	9.04×10^6	0.0245	1.53×10^7	0.021	2.16×10^7	0.0055
3.01×10^6	0	9.29×10^6	0.0255	1.56×10^7	0.0205	2.19×10^7	0.005
3.27×10^6	0	9.55×10^6	0.026	1.58×10^7	0.0195	2.21×10^7	0.005
3.52×10^6	0	9.80×10^6	0.026	1.61×10^7	0.019	2.24×10^7	0.0045
3.77×10^6	0	1.00×10^7	0.0265	1.63×10^7	0.0185	2.26×10^7	0.0045
4.02×10^6	0	1.03×10^7	0.0265	1.66×10^7	0.0175	2.29×10^7	0.0045
4.27×10^6	0	1.06×10^7	0.027	1.68×10^7	0.017	2.31×10^7	0.004
4.52×10^6	0	1.08×10^7	0.027	1.71×10^7	0.0165	2.34×10^7	0.004
4.77×10^6	0	1.11×10^7	0.027	1.73×10^7	0.0155	2.36×10^7	0.004
5.02×10^6	0	1.13×10^7	0.027	1.76×10^7	0.015	2.39×10^7	0.004
5.28×10^6	0	1.16×10^7	0.027	1.78×10^7	0.0145	2.41×10^7	0.0035
5.53×10^6	0	1.18×10^7	0.0265	1.81×10^7	0.0135	2.44×10^7	0.0035
5.78×10^6	0.0035	1.21×10^7	0.0265	1.83×10^7	0.013	2.46×10^7	0.0035
6.03×10^6	0.0065	1.23×10^7	0.0265	1.86×10^7	0.012	2.49×10^7	0.0035
6.28×10^6	0.009	1.26×10^7	0.026	1.88×10^7	0.0115	2.51×10^7	0.0035

combined with models of particle aggregation dynamics (e.g., Burd and Jackson 2009) to assess more complex suites of particle characteristics.

The concentration of particles, N_p, (number m^{-3}), which is used to convert between individual particle concentrations and the concentration for all particles per volume seawater, is based on measurements from Iversen et al. (2010).

$$N_p = \frac{\text{POM}}{W_{\text{dry}} R_{C:W_{\text{dry}}}} \tag{A10}$$

where POM is the concentration of particulate organic matter (mg m^{-3}), W_{dry} is the dry weight of an individual particle (mg), and $R_{C:W_{\text{dry}}}$ is the mg carbon to mg particle dry

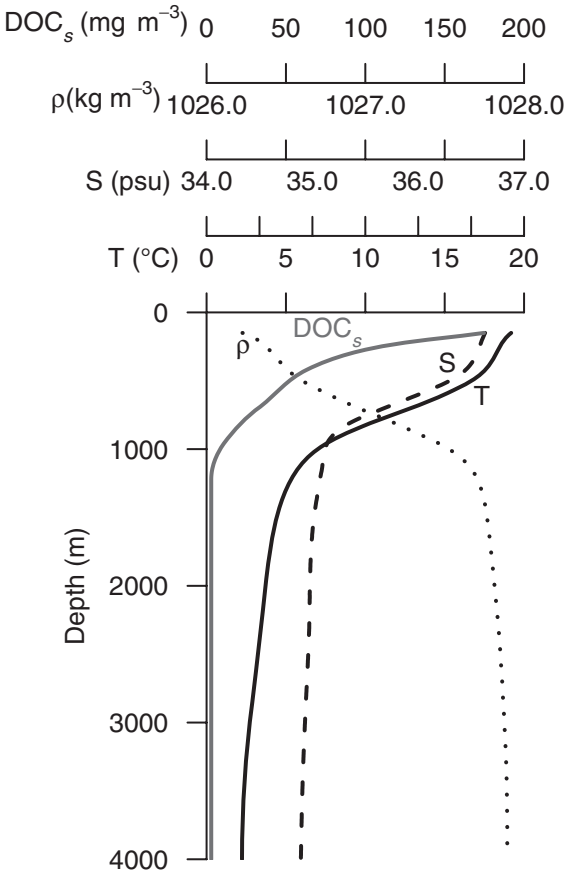

Figure A1. Vertical profiles used in the model. The gray solid line is semilabile dissolved organic carbon, DOC$_s$; the black dotted line is density, ρ; the black dashed line is salinity, S; and the black solid line is temperature, T.

weight conversion ratio. Particle dry weight in mg, W_{dry}, is determined using an empirical relationship with particle radius r (mm) from Iversen et al. (2010).

$$W_{\text{dry}} = 15000r^{1.8} \tag{A11}$$

The volume of an individual particle, V_p, is also used to convert between particle and total concentrations. The particles were assumed to be spherical in shape so the standard geometric relationship was used to calculate V_p,

$$V_p = \frac{4}{3}\pi r^3 \tag{A12}$$

where r is the radius of the particle.

c. Bacterial uptake and growth

The model includes two functional groups of heterotrophic bacteria, a free-living group, DB, and an attached group, PB. The formulations used to calculate uptake and growth are commonly used in ecosystem models (reviewed in Flynn 2005). The growth rate coefficient of free-living bacteria, μ_{DB}, depends on the maximum growth efficiency, B_{GEmax}, nutrient uptake in h^{-1}, v_{DB}, and basal metabolic rate in h^{-1}, Υ,

$$\mu_{DB} = B_{GEmax} v_{DB} - \Upsilon \tag{A13}$$

B_{GEmax} (dimensionless) is the ratio of uptake available for growth relative to the total amount of uptake for growth and respiration. Υ is the minimum nutrient requirement for bacterial survival in an inactive state. v_{DB} in the following equation is determined using Michaelis-Menten kinetics:

$$v_{DB} = v_{max} \left(\frac{HD}{k_{HD} + HD} \right) \tag{A14}$$

The parameters are symbolized by v_{max} and k_{HD} for maximum uptake rate in h^{-1} and half saturation constant in mg m^{-3} seawater respectively. HD is the concentration of dissolved hydrolysate in mg m^{-3} seawater.

The achieved bacterial growth efficiency is calculated as follows:

$$B_{GE} = \frac{\mu_{DB}}{v_{DB}} \tag{A15}$$

All carbon substrates not used for growth (1-B_{GE})v_{DB} are remineralized.

The equation to calculate μ_{PB}, growth of PB, is similar to the equation for μ_{DB} but includes an additional term for exoenzymes ϵ in units of h^{-1},

$$\mu_{PB} = B_{GEmax} v_{PB} - \Upsilon - \epsilon \tag{A16}$$

The basal metabolic rate constant (Υ, h^{-1}), bacterial growth efficiency (B_{GEmax}, dimensionless), and maximum nutrient uptake rate constant (v_{max}, h^{-1}) are the same for DB and PB. Uptake by PB is scaled for the particle using the concentration of hydrolysate per unit volume of particle HP_p in mg m^{-3} particle:

$$v_{PB} = v_{max} \left(\frac{HP_p}{k_{HP} + HP_p} \right) \tag{A17}$$

where k_{HP} is the uptake half-saturation constant for hydrolysate in particles in mg m^{-3} particle, which is also a particle-based concentration. HP_p and k_{HP} are used in a dimensionless fraction in equation (A17). The dimensionless fraction makes it possible for v_{PB} to be relevant for the total concentration of PB in mg m^{-3} seawater, but scaled for the elevated concentration of HP surrounding PB in a particle. The equation to calculate HP_p is

$$HP_p = \frac{HP}{N_p V_p} \tag{A18}$$

where HP is the concentration of hydrolysate in the particle in mg m^{-3}, N_p is the number of particles per m^{-3} from equation (A10), and V_p is the volume in m^3 of each particle from equation (A12).

For the *Interception* scenario, ν_{PB} is a portion the hydrolysate diffusing out of the particle, so the particle-attached bacteria are utilizing hydrolysate that otherwise would be lost from the particle. Therefore, in the model, ν_{PB} is subtracted from $\Theta q_{HP}(HP_p - HD)$ rather than being considered an independent term in equation (A6). Likewise, in equation (A7), the amount of hydrolysate diffusing out of the particle to become dissolved hydrolysate is only the fraction that bacteria do not take up.

Exoenzyme production in h^{-1}, ϵ, is related to particle-attached bacterial abundance and is based on optimal particle-attached bacterial production, the exoenzyme production rates with the highest particle-attached bacterial production. Exoenzyme production was derived from an optimization analysis of the model because there are many unknowns in how quorum sensing results in the production of exoenzymes in particles. In order to focus on particle-based processes in the optimization analysis, there was no attachment of free-living bacteria, $\beta = 0$. The temperature, salinity, and density of seawater in the optimization analysis were 20°C, 36.6 psu, and 1026 kg m^{-3} respectively. Optimal particle-attached bacterial production was determined by simultaneously varying exoenzyme production, ϵ, between 0 and 0.05 h^{-1} and initial particle-attached bacterial abundance between 2.51×10^5 and 2.76×10^7. The exoenzyme concentration that resulted in the greatest particle-attached bacterial production (i.e., "optimal" ϵ) was plotted versus initial particle-attached bacterial abundance to determine the functional form of equation (A19) for the *Interior* and *Interception* scenarios.

$$PB_p > \theta_\epsilon;\ \epsilon = \epsilon_{max}\left(\frac{(PB_p - \theta_\epsilon)^x}{(k_\epsilon - \theta_\epsilon)^x + (PB_p - \theta_\epsilon)^x}\right)$$

$$PB_p \leq \theta_\epsilon;\ \epsilon = 0 \tag{A19}$$

ϵ_{max} is the maximum exoenzyme production rate (h^{-1}). PB_p is mg C of particle-attached bacteria per particle. θ_ϵ is the particle-attached bacterial biomass threshold for inception of exoenzyme production (mg C $particle^{-1}$). k_ϵ is the half production constant for particle-attached bacterial biomass (mg C $particle^{-1}$), and x is a fitted exponent. Parameters are given in Table A2.

In equation (A19), concentrations per particle, PB_p, θ_ϵ, and k_ϵ, are used in a dimensionless ratio to scale exoenzyme production for the total homogenized concentration of bacteria, PB in mg m^{-3} seawater. The calculation for PB_p is

$$PB_p = \frac{PB}{N_p} \tag{A20}$$

where PB is the concentration of particle-attached bacteria mg m^{-3} seawater and N_p is the number of particles per volume of seawater calculated in equation (A10). Note that PB_p has different units (mg C per particle) than HP_p (mg C per m^{-3} particle) in equation (A18).

A lookup table is used to determine ϵ using PB_p for the *Retention* scenario when particle-attached bacteria retain hydrolysate and exoenzyme in the particle (Table A3).

d. Ecological interactions

Cooperation and/or competition may develop as bacterial populations increase in size. On particles in the model, these ecological interactions are determined by particle surface area, which is limited. For calculating the retention of solutes in the *Retention* scenario and competition for all the scenarios, the model uses the number of particle-attached bacteria needed to cover the surface area of a particle in a single layer. For *Retention*, the model assumption is that the bodies of the particle-attached bacteria prevent the diffusion of solute out of the particle in proportion to coverage of the particle. For competition, the model assumption is that particle-attached bacteria repel new colonizers and disperse new cells relative to the coverage of the particle. B_{pA} is the abundance of particle-attached bacteria needed to cover the entire surface of a particle, which is calculated as the surface area of spherical particle divided by the "footprint" of a single particle-attached bacterium,

$$B_{pA} = \frac{4\pi r^2}{l_B d_B} \tag{A21}$$

where r is radius of the particle, l_B is the length of a rod-shaped bacterium, and d_B is the diameter of a rod-shaped bacterium. In the *Interior* scenario, B_{pA} refers to a threshold at which particle-attached bacteria are at high population densities rather than the threshold at which the particle is completely covered by particle-attached bacteria.

e. Bacterial attachment

Organic nutrients are sparse in the deep ocean making particles a rich resource. In order to access the nutrients, bacteria must first attach to the particles. The attachment rate constant, β, is based on the colonization model of Kiørboe et al. (2002). The Kiørboe et al. (2002) model was selected because it bases diffusivity on measurements including swimming speed, run length, and turning angle of random walk behavior, which is used by free-living bacteria to find nutrient resources in aquatic environments (Berg 1993). Chemotaxis (e.g., Stocker and Seymour 2012) is not yet included. The equation for β is

$$\beta = 4\pi D r \underline{Sh} N_p \tag{A22}$$

where D is the diffusivity of randomly walking bacteria in $m^2\ h^{-1}$, r is the radius of the particle in m, and $\underline{Sh}$ is the dimensionless Sherwood number. The Kiørboe et al. (2002) attachment rate constant is for a single particle. Total attachment for all particles is calculated by multiplying by N_p, the number of particles per m^{-3} seawater.

The Sherwood number $\underline{Sh}$ is the ratio between total mass transfer and transfer due to diffusion alone (Kiørboe, Ploug, and Thygesen 2001). Thus, it serves to include both advection

and diffusion as part of the attachment calculation.

$$\underline{Sh} = 1 + 0.619\underline{Re}^{0.412}\left(\frac{\nu}{D}\right)^{1/3} \tag{A23}$$

where ν is kinematic viscosity in $m^2\ h^{-1}$, and D is the diffusivity of randomly walking bacteria in $m^2\ h^{-1}$ (Kiørboe et al. 2002). The dimensionless Reynold's number, $\underline{Re}$, is the ratio of inertial to viscous forces,

$$\underline{Re} = \frac{wr}{\nu} \tag{A24}$$

where w is the sinking speed of the particle in m h^{-1}, r is the radius of the particle in m, and ν is the kinematic viscosity in $m^2\ h^{-1}$.

The diffusivity, D, is needed for equations (A22) and (A23) and is based on the utilization of random walk behavior by free-living bacteria (Kiørboe et al. 2002),

$$D = \frac{u^2\tau}{6(1-\alpha)} \tag{A25}$$

where u is free-living bacterial swimming speed in m h^{-1}, τ is run length in h, and α is the cosine of the angle between runs.

f. Bacterial detachment

Kiørboe et al. (2002) found it necessary to include a detachment rate in order to correctly predict bacterial abundance on particles using the colonization model. Bacterial detachment was quantified in a subsequent study, which also found that there were varying degrees in ability to detach (Kiørboe et al. 2003). We incorporated a mechanistic detachment rate in the model making the assumption that negative interactions, especially competition, between bacteria are a factor that determines whether particle-attached bacteria detach from particles (Grossart et al. 2003). The detachment rate constant δ depends on the space available on the outer surface of the particle.

$$\delta = \delta_{max}\left(\frac{\mathrm{PB}_p}{B_{pA}R_{C:B} + \mathrm{PB}_p}\right) \tag{A26}$$

δ_{max} is the maximum detachment rate in h^{-1}. PB_p is mg of bacteria per particle. B_{pA} is the number of particle-attached bacteria needed to cover the outer surface of a particle from equation (A21). $R_{C:B}$ is mg of carbon per bacterium. Competition on the particle depends on bacterial concentration on a particle. Detachment, δ, is for the homogenized concentration of particle-attached bacteria, but is scaled using the dimensionless ratio that incorporates the particle-based concentration, PB_p.

An assumption of the model is that detachment occurs due to competition. Competition occurs when particle-attached bacteria exceed single-layer particle coverage, B_{pA}. The maximum detachment rate constant, δ_{max}, when competition is occurring ($\mathrm{PB}_p \geq B_{pA}$) is based

on new growth μ_{PB} (h^{-1}) and attachment rates β (h^{-1}) and functions to increase dispersal and decrease new colonization. New colonizers are in the process of attaching but not actually attached, so β is multiplied by DB/PB to account for colonizers that are in the process of attaching.

$$\mathrm{PB}_p \geq B_{pA} \rightarrow \delta_{max} = \mu_{\mathrm{PB}} + \frac{\beta \mathrm{DB}}{\mathrm{PB}} \tag{A27}$$

$$\mathrm{PB}_p < B_{pA} \rightarrow \delta_{max} = 0 \tag{A28}$$

g. Exoenzyme activity

Particle-attached bacteria produce exoenzymes (equations A16, A19) in order to cleave hydrolysate molecules small enough to be transported into the cell. Exoenzyme activity is assumed to depend on the ratio of the amount of particulate organic matter available (POM − Γ) to the total particulate organic matter (POM). When POM is sufficiently abundant, exoenzyme activity, γ in h^{-1}, hydrolyzes substrates at maximum rates, γ_{max}, but as a larger fraction of POM is shielded by inorganic materials, exoenzymes likely become less efficient decreasing activity rates. Armstrong et al. (2002) found that ballast in particles "protects" organic material from degradation, so in the model, we use ballast to calculate the protected material Γ in mg C m^{-3}.

$$\gamma = \max\left(0, \gamma_{max}\left(\frac{\mathrm{POM} - \Gamma}{\mathrm{POM}}\right)\right) \tag{A29}$$

Ballast, Γ, consists of calcium carbonate, opal, and lithogenic material from terrestrial dust, and the fractions of organic carbon protected relative to quantity of each ballast component, $f_{\mathrm{CaCO_3}}$, f_{opal}, and f_{lith}, have been measured in a global analysis of sediment traps (Klaas and Archer 2002).

$$\Gamma = \frac{f_{\mathrm{CaCO_3}}\Phi_{\mathrm{CaCO_3}} + f_{opal}\Phi_{opal} + f_{lith}\Phi_{lith}}{w} \tag{A30}$$

$\Phi_{\mathrm{CaCO_3}}$, Φ_{opal}, and Φ_{lith} are the fluxes of calcium carbonate, opal, and lithogenic material in mg m^2 h^{-1}, and w is sinking speed in m h^{-1}.

h. Mass transfer

Hydrolysate, HP, and exoenzymes, EP and XP, accumulate inside the particle as it is sinking and diffuse and advect, cumulatively referred to as mass transfer, out of the particle to the dissolved environment. The mass transfer coefficient in m^3 h^{-1} for hydrolysate, q_{H}, between a particle and the external environment is based on an equation from Ploug (2001),

$$q_{\mathrm{H}} = 4\pi r D_{\mathrm{H}} \underline{Sh} N_p \tag{A31}$$

where r is the radius of the particle in m, D_{H} is the diffusivity of hydrolysate in m^2 h^{-1}. $\underline{Sh}$ is the dimensionless Sherwood number. The mass transfer coefficient from Ploug (2001) is

for the entire surface area of a single particle. It is multiplied by N_p, the number of particles per m^{-3} seawater, to get the total transfer for the homogenized concentration of hydrolysate, HP. D_E is substituted for D_H to convert equation (A31) for q_{EP} and q_{XP}.

The Stokes-Einstein equation as described in Jumars et al. (1993) is used to determine D_H.

$$D_H = \frac{k_b T}{6\pi\eta r_H} \tag{A32}$$

where k_b is the Boltzman constant in kg m^{-2} s^{-1} K^{-1}. T is temperature in kelvin (K). η is dynamic viscosity in kg m^{-1} s^{-1}, and r_H is the radius of a hydrolysate molecule in m. To calculate D_E for exoenzyme, r_E, the radius of exoenzyme molecules, is substituted for r_H.

The fitted relation for the dimensionless Sherwood number, $\underline{Sh}$ calculated by Kiørboe, Ploug, and Thygesen (2001) from measurements, is used to quantify advective transfer related to the downward sinking of the particle.

$$\underline{Sh} = 1 + 0.619\underline{Re}^{0.412}\underline{Sc}^{1/3} \tag{A33}$$

$\underline{Re}$ is the dimensionless Reynold's number (see equation A24), and $\underline{Sc}$ is the dimensionless Schmidt number (Kiørboe et al. 2001),

$$\underline{Sc} = \frac{\nu}{D_H} \tag{A34}$$

where ν is kinematic viscosity in m^2 h^{-1} and D_H is diffusivity of hydrolysate as calculated in equation (A32).

Fluxes of HP, EP, and XP from the particle are determined by multiplying q_H and q_E (equation A31) by the concentration difference between the particle and dissolved environments. The concentration in a particle is determined by converting HP, EP, and XP to particle-based concentrations. HP_p, the particle-based concentration for HP, is calculated in equation (A18). The concentrations of EP and XP in the particle, EP_p and XP_p, are calculated in the following text. The concentration differences, $(HP_p - HP)$, $(EP_p - EP)$, and $(XP_p - XP)$, are used in the governing equations (equations A4–A9).

The calculation of EP_p includes some additional terms because active exoenzyme, EP, does not freely diffuse while bound to substrates. The effect of binding increases as the fraction of binding sites, which are directly proportional to the amount of substrate available, increases. Bound exoenzyme is excluded from the calculations of mass transfer by using volume of substrate V_M in m^3 relative to the total particle volume V_p in m^3 divided by the total particle volume V_p in a dimensionless fraction. EP_p is the actively diffusing exoenzyme per m^{-3} of particle.

$$EP_p = \frac{EP(V_p - V_M)}{V_p^2 N_p} \tag{A35}$$

EP is divided by V_p and N_p to convert from mg m^{-3} of seawater to the particle-based concentration of mg m^{-3} particle.

The volume of substrate in a particle, V_M, is calculated from the substrate density ρ_M, in g cm^{-3}.

$$V_M = \max\left(0, \frac{R_{M:C}\mathrm{POM}\left(\frac{\mathrm{POM}-\Gamma}{\mathrm{POM}}\right)}{N_p \rho_M}\right) \tag{A36}$$

$R_{M:C}$ is mg substrate per mg C within the substrate. POM is particulate carbon in mg C m^{-3} seawater. Γ is the carbon protected by ballast in mg C m^{-3} seawater (equation A21). The volume of substrate in a single particle, V_M, is determined by dividing the total volume of substrate in all particles by N_p, the number of particles per m^{-3} of seawater.

Inactive exoenzyme XP freely diffuses within the particle. XP_p is inactive exoenzyme per m^{-3} particle.

$$\mathrm{XP}_p = \frac{\mathrm{XP}}{N_p V_p} \tag{A37}$$

N_p is the number of particles per m^{-3} of seawater (equation A10). V_p is volume of a particle (equation A12).

Fluxes of HP, EP, and XP from the particle are modified by an additional term in the *Retention* scenario. Bacteria cells form a physical barrier, represented by a fraction Θ, that prevent diffusion and advection, q from equation (A31), of solutes, HP, EP, and XP, when bacterial abundance is high.

$$\Theta = \max\left(0, 1 - \frac{\mathrm{PB}_p}{B_{pA} R_{C:B}}\right) \tag{A38}$$

PB_p is the mg of bacteria per particle (equation A20). B_{pA} is the number of bacteria to cover the particle in a single layer (equation A21). $R_{C:B}$ is the fg of carbon per bacterium. All solutes are retained in particles when bacterial coverage exceeds 100%, i.e., $\mathrm{PB}_p > B_{pA} R_{C:B}$. Solutes are fractionally retained in the particles depending on abundance when coverage is <100%. For the *Interior* and *Interception* scenarios, $\Theta = 1$.

The model has both active and inactive exoenzymes. Active exoenzymes, EP, have a limited lifetime, and the exoenzyme deactivation rate constant m_E in h^{-1} is calculated using a half-life $t_{1/2}$ in h (Steen and Arnosti 2011).

$$m_\mathrm{E} = -\frac{\ln(0.5)}{t_{1/2}} \tag{A39}$$

i. Bacterial mortality

Sources of mortality for bacteria include predation by flagellates, viral lysis, and natural senescence. Particles, which have highly concentrated organic biomass, and the dissolved

environment have different characteristics: There are higher abundances of predatory flagellates on particles, and viral abundances tend to be higher in denser bacterial communities (Maranger and Bird 1995; Kiørboe et al. 2003). Viruses in particles collected from sediment traps were found clustered in aggregations suggesting a potential virus concentrating mechanism in the particle environment; however, the impact clustering has on infection and lysing rates is unknown (Proctor and Fuhrman 1991). These studies suggest that the mortality coefficient is higher for particle-attached bacteria, PB, than for free-living bacteria, DB. In the microbial remineralization model, all sources of mortality, including natural senescence, are combined into a single quadratic mortality term. For PB, the mortality coefficient, m_{PB}, is approximated to be twice the mortality coefficient, m_{DB}, of DB (Table A1).

j. Dissolved organic carbon

DOC is found in relatively high concentrations in the deep ocean, but only a small fraction is available for consumption by heterotrophic bacteria (Hansell 2013). Refractory DOC, DOC_r, breaks down over century to millennial timescales and so does not significantly contribute to bacterial food sources on a daily basis (Hansell 2013). However, semilabile DOC, DOC_s, decays on a much faster timescale, $\leq$5 years, and needs to be considered as a food source for bacteria living in the deep ocean (Hansell 2013). DOC_s is supplied to deeper depths through deep mixing and large-scale ocean circulation (Carlson et al. 1994; Hansell and Carlson 2001), physical processes not included in this model. A DOC_s profile in mg m^{-3} (shown in Fig. A1) is derived by subtracting long-term averages of DOC from below 1,000 m, considered to be DOC_r, from profiles of DOC (Hansell and Carlson 2001).

$$DOC_s = DOC - DOC_r \tag{A40}$$

In the microbial remineralization model, DOC_s decays at a constant rate, κ, per unit time, to HD,

$$\kappa = \frac{1}{t_{DOC}} \tag{A41}$$

where t_{DOC} is the decay timescale in h^{-1}.

k. Temperature dependence

Temperature varies with depth in the water column (Fig. A1). Temperature dependence is incorporated in the calculation of kinematic viscosity and the diffusion coefficients (Fig. A1) (Jumars et al. 1993). Additionally, the nutrient uptake rate constant, exoenzyme activity rate constant, and exoenzyme lifetime are temperature dependent. We model the temperature dependence of these biological rates using Q_{10} scaling, a measure of rate changes relative to a 10°C change in temperature. Note that higher temperatures increase activity rates and decrease lifetimes. The rates that are scaled for temperature are indicated by an asterisk in the model parameters (Table A1).

REFERENCES

Abell, J., S. Emerson, and P. Renaud. 2000. Distributions of TOP, TON and TOC in the North Pacific subtropical gyre: Implications for nutrient supply in the surface ocean and remineralization in the upper thermocline. J. Mar. Res., *58*, 203–222.

Alldredge, A. L. 1979. The chemical composition of macroscopic aggregates in two neritic seas. Limnol. Oceanogr., *24*, 855–866.

Alldredge, A. L., and C. Gotschalk. 1988. In situ settling behavior of marine snow. Limnol. Oceanogr., *33*, 339–351.

Aluwihare, L. I., D. J. Repeta, S. Pantoja, and C. G. Johnson. 2005. Two chemically distinct pools of organic nitrogen accumulate in the ocean. Science, *308*, 1007–1010.

Antia, A. N. 2005. Solubilization of particles in sediment traps: Revising the stoichiometry of mixed layer export. Biogeosciences, *2*, 189–204.

Armstrong, R. A., C. Lee, J. I. Hedges, S. Honjo, and S. G. Wakeham. 2002. A new, mechanistic model for organic carbon fluxes in the ocean based on the quantitative association of POC with ballast minerals. Deep-Sea Res., Part II, *49*, 219–236.

Arnosti, C. 2011. Microbial extracellular enzymes and the marine carbon cycle. Annu. Rev. Mar. Sci., *3*, 401–425.

Azam, F., and F. Malfatti. 2007. Microbial structuring of marine ecosystems. Nat. Rev. Microbiol., *5*, 782–791.

Baltar, F., J. Arístegui, J. M. Gasol, E. Sintes, H. M. van Aken, and G. J. Herndl. 2010. High dissolved extracellular enzymatic activity in the deep central Atlantic Ocean. Aquat. Microb. Ecol., *58*, 287–302.

Baltar, F., J. Arístegui, J. M. Gasol, T. Yokokawa, and G. J. Herndl. 2013. Bacterial versus archaeal origin of extracellular enzymatic activity in the Northeast Atlantic deep waters. Microb. Ecol., *65*, 277–288.

Baltar, F., J. Arístegui, E. Sintes, H. M. van Aken, J. M. Gasol, and G. J. Herndl. 2009. Prokaryotic extracellular enzymatic activity in relation to biomass production and respiration in the meso- and bathypelagic waters of the (sub)tropical Atlantic. Environ. Microbiol.,11, 1998–2014.

Berg, H. C. 1993. Random Walks in Biology. Princeton, NJ: Princeton University Press, 168 pp.

Bishop, J. K. B., J. M. Edmond, D. R. Ketten, M. P. Bacon, and W. B. Silker. 1977. The chemistry, biology, and vertical flux of particulate matter from the upper 400 m of the equatorial Atlantic Ocean. Deep-Sea Res., *24*, 511–520.

Buesseler, K. O., A. N. Antia, M. Chen, S. W. Fowler, W. D. Gardner, O. Gustafsson, K. Harada, et al. 2007. An assessment of the use of sediment traps for estimating upper ocean particle fluxes. J. Mar. Res., *65*, 345–416.

Buitenhuis, E., W. K. W. Li, M. W. Lomas, D. M. Karl, M. R. Landry, and S. Jacquet. 2012. Pico-heterotroph (*Bacteria* and *Archaea*) biomass distribution in the global ocean. Earth Syst. Sci. Data, *4*, 101–106.

Burd, A. B., and G. A. Jackson. 2009. Particle aggregation. Annu. Rev. Mar. Sci., *1*, 65–90.

Burley, S. K., P. R. David, A. Taylor, and W. N. Lipscomb. 1990. Molecular structure of leucine aminopeptidase at 2.7-Å resolution. Proc. Natl. Acad. Sci. U. S. A., *87*, 6878–6882.

Carlson, C. A., H. W. Ducklow, and A. F. Michaels. 1994. Annual flux of dissolved organic carbon from the euphotic zone in the northwestern Sargasso Sea. Nature, *371*, 405–408.

Christian, J. R., and T. R. Anderson. 2002. Modeling DOM biogeochemistry, *in* Biogeochemistry of Marine Dissolved Organic Matter, D. A. Hansell and C. A. Carlson, eds. New York. Plenum Press, 717–755.

Conte, M. H., N. Ralph, and E. H. Ross. 2001. Seasonal and interannual variability in deep ocean particle fluxes at the Oceanic Flux Program (OFP)/Bermuda Atlantic Time Series (BATS) site in the western Sargasso Sea near Bermuda. Deep-Sea Res., Part II, *48*, 1471–1505.

del Giorgio, P. A., and J. J. Cole. 2000. Bacterial energetics and growth efficiency, *in* Microbial Ecology of the Oceans, D. L. Kirchman, ed. New York: Wiley-Liss, 289–325.

Dell, A. I., S. Pawar, and V. M. Savage. 2011. Systematic variation in the temperature dependence of physiological and ecological traits. Proc. Natl. Acad. Sci. U. S. A., *108*, 10591–10596.

Drescher, K., C. D. Nadell, H. A. Stone, N. S. Wingreen, and B. L. Bassler. 2014. Solutions to the public goods dilemma in bacterial biofilms. Curr. Biol., *24*, 50–55.

Duhamel, S., S. T. Dyhrman, and D. M. Karl. 2010. Alkaline phosphatase activity and regulation in the North Pacific Subtropical Gyre. Limnol. Oceanogr., *55*, 1414–1425.

Flynn, K. J. 2005. Incorporating plankton respiration in models of aquatic ecosystem function, *in* Respiration in Aquatic Systems, P. A. del Giorgio and P. J. le B. Williams, eds. Oxford: Oxford University Press, 248–266.

Giering, S. L., R. Sanders, R. S. Lampitt, T. R. Anderson, C. Tamburini, M. Boutrif, M. V. Zubkov, et al. 2014. Reconciliation of the carbon budget in the ocean's twilight zone. Nature, *507*, 480–483.

Gram, L., H.-P. Grossart, A. Schlingloff, and T. Kiørboe. 2002. Possible quorum sensing in marine snow bacteria: Production of acylated homoserine lactones by *Roseobacter* strains isolated from marine snow. Appl. Environ. Microbiol., *68*, 4111–4116.

Grossart, H.-P., T. Kiorboe, K. Tang, and H. Ploug. 2003. Bacterial colonization of particles: Growth and interactions. Appl. Environ. Microbiol., *69*, 3500–3509.

Gundersen, K., M. Heldal, S. Norland, D. A. Purdie, and A. H. Knap. 2002. Elemental C, N, and P cell content of individual bacteria collected at the Bermuda Atlantic Time-series Study (BATS) site. Limnol. Oceanogr., *47*, 1525–1530.

Hannides, A. K., S. M. Dunn, and R. C. Aller. 2005. Diffusion of organic and inorganic solutes through macrofaunal mucus secretions and tube linings in marine sediments. J. Mar. Res., *63*, 957–981.

Hansell, D. A. 2013. Recalcitrant dissolved organic carbon fractions. Ann. Rev. Mar. Sci., *5*, 421–445.

Hansell, D. A., and C. A. Carlson. 2001. Biogeochemistry of total organic carbon and nitrogen in the Sargasso Sea: Control by convective overturn. Deep-Sea Res., Part II, *48*, 1649–1667.

Haynes, W. M., ed. 2012. Physical constants of organic compounds, *in* CRC Handbook of Chemistry and Physics, 93rd ed. Boca Raton, FL: CRC Press/Taylor and Francis.

Herndl, G. J., and T. Reinthaler. 2013. Microbial control of the dark end of the biological pump. Nat. Geosci., *6*, 718–724.

Herndl, G. J., T. Reinthaler, E. Teira, H. van Aken, C. Veth, A. Pernthaler, and J. Pernthaler. 2005. Contribution of *Archaea* to total prokaryotic production in the deep Atlantic Ocean. Appl. Environ. Microbiol., *71*, 2303–2309.

Hmelo, L. R., T. J. Mincer, and B. A. S. Van Mooy. 2011. Possible influence of bacterial quorum sensing on the hydrolysis of sinking particulate organic carbon in marine environments. Environ. Microbiol. Rep., *3*, 682–688.

Honjo, S., and M. R. Roman. 1978. Marine copepod fecal pellets: Production, preservation, and sedimentation. J. Mar. Res., *36*, 45–57.

Hoppe, H. G., C. Arnosti, and G. F. Herndl. 2002. Ecological significance of bacterial enzymes in the marine environment, *in* Enzymes in the Environment: Activity, Ecology, and Applications, R. G. Burns and R. P. Dick, eds. New York: Marcel Dekker.

Iversen, M. H., N. Nowald, H. Ploug, G. A. Jackson, and G. Fischer. 2010. High resolution profiles of vertical particulate organic matter export off Cape Blanc, Mauritania: Degradation processes and ballasting effects. Deep-Sea Res., Part I, *57*, 771–784.

Jacobsen, T. R., and F. Azam. 1984. Role of bacteria in copepod fecal pellet decomposition: Colonization, growth-rates and mineralization. Bull. Mar. Sci., *35*, 495–502.

Jing, H., L. Shek, W. Yung, X. Jin, and H. Liu. 2012. Dynamics of bacterial community composition during degradation of copepod fecal pellets. J. Plankton Res., *34*, 700–710.

Jumars, P. A., J. W. Deming, P. S. Hill, L. Karp-Boss, P. L. Yager, and W. B. Dade. 1993. Physical constraints on marine osmotrophy in an optimal foraging context. Mar. Microb. Food Webs, *7*, 121–159.

Jumars, P. A., D. L. Penry, J. A. Baross, M. J. Perry, and B. W. Frost. 1989. Closing the microbial loop: Dissolved carbon pathway to heterotrophic bacteria from incomplete ingestion, digestion, and absorption in animals. Deep-Sea Res., Part A, *36*, 483–495.

Karner, M., and G. J. Herndl. 1992. Extracellular enzymatic-activity and secondary production in free-living and marine-snow-associated bacteria. Mar. Biol., *113*, 341–347.

Kiørboe, T., H.-P. Grossart, H. Ploug, and K. Tang. 2002. Mechanisms and rates of bacterial colonization of sinking aggregates. Appl. Environ. Microbiol., *68*, 3996–4006.

Kiørboe, T., H. Ploug, and U. H. Thygesen. 2001. Fluid motion and solute distribution around sinking aggregates. I. Small-scale fluxes and heterogeneity of nutrients in the pelagic environment. Mar. Ecol. Prog. Ser., *211*, 1–13.

Kiørboe, T., K. Tang, H.-P. Grossart, and H. Ploug. 2003. Dynamics of microbial communities on marine snow aggregates: Colonization, growth, detachment, and grazing mortality of attached bacteria. Appl. Environ. Microbiol., *69*, 3036–3047.

Kirchman, D. L. 2012. Processes in Microbial Ecology. Oxford: Oxford University Press, 328 pp.

Klaas, C., and D. E. Archer. 2002. Association of sinking organic matter with various types of mineral ballast in the deep sea: Implications for the rain ratio. Global Biogeochem. Cycles,16, 1116.

Kwon, E. Y., F. Primeau, and J. L. Sarmiento. 2009. The impact of remineralization depth on the air-sea carbon balance. Nat. Geosci., *2*, 630–635.

Li, W. K. W., and W. G. Harrison. 2001. Chlorophyll, bacteria and picophytoplankton in ecological provinces of the North Atlantic. Deep-Sea Res., Part II, *48*, 2271–2293.

Lutz, M., R. Dunbar, and K. Caldeira. 2002. Regional variability in the vertical flux of particulate organic carbon in the ocean interior. Global Biogeochem. Cycles, *16*, 1037.

Maranger, R., and D. F. Bird. 1995. Viral abundance in aquatic systems: A comparison between marine and fresh waters. Mar. Ecol. Prog. Ser., *121*, 217–226.

Martin, J. H., G. A. Knauer, D. M. Karl, and W. W. Broenkow. 1987. VERTEX: Carbon cycling in the northeast Pacific. Deep-Sea Res., Part A, *34*, 267–285.

Miller, M. B., and B. L. Bassler. 2001. Quorum sensing in bacteria. Annu. Rev. Microbiol., *55*, 165–199.

Müller-Niklas, G., S. Schuster, E. Kaltenböck, and G. Herndl. 1994. Organic content and bacterial metabolism in amorphous aggregates of the northern Adriatic Sea. Limnol. Oceanogr., *39*, 58–68.

Nagasawa, S., and T. Nemoto. 1988. Presence of bacteria in guts of marine crustaceans and on their fecal pellets. J. Plankton Res., *10*, 559–564.

Orellana, M. V., and D. A. Hansell. 2012. Ribulose-1,5-bisphosphate carboxylase/oxygenase (RuBisCO): A long-lived protein in the deep ocean. Limnol. Oceanogr., *57*, 826–834.

Ploug, H. 2001. Small-scale oxygen fluxes and remineralization in sinking aggregates. Limnol. Oceanogr., *46*, 1624–1631.

Proctor, L. M., and J. A. Fuhrman. 1991. Roles of viral infection in organic particle flux. Mar. Ecol. Prog. Ser., *69*, 133–142.

Rawn, J. D. 1989. Biochemistry. Burlington, NC: Neil Patterson.

Smith, D. C., M. Simon, A. L. Alldredge, and F. Azam. 1992. Intense hydrolytic enzyme activity on marine aggregates and implications for rapid particle dissolution. Nature, *359*, 139–142.

Steen, A. D., and C. Arnosti. 2011. Long lifetimes of β-glucosidase, leucine aminopeptidase, and phosphatase in Arctic seawater. Mar. Chem., *123*, 127–132.

Steinberg, D. K., C. A. Carlson, N. R. Bates, R. J. Johnson, A. F. Michaels, and A. H. Knap. 2001. Overview of the US JGOFS Bermuda Atlantic Time-series Study (BATS): A decade-scale look at ocean biology and biogeochemistry. Deep-Sea Res., Part II, *48*, 1405–1447.

Stocker, R., and J. R. Seymour. 2012. Ecology and physics of bacterial chemotaxis in the ocean. Microbiol. Mol. Biol. Rev., *76*, 792–812.

Teira, E., P. Lebaron, H. van Aken, and G. J. Herndl. 2006. Distribution and activity of Bacteria and Archaea in the deep water masses of the North Atlantic. Limnol. Oceanogr., *51*, 2131–2144.

Vetter, Y. A., J. W. Deming, P. A. Jumars, and B. B. Krieger-Brockett. 1998. A predictive model of bacterial foraging by means of freely released extracellular enzymes. Microb. Ecol., *36*, 75–92.

West, S. A., K. Winzer, A. Gardner, and S. P. Diggle. 2012. Quorum sensing and the confusion about diffusion. Trends Microbiol., *20*, 586–594.

Ziervogel, K., A. D. Steen, and C. Arnosti. 2010. Changes in the spectrum and rates of extracellular enzyme activities in seawater following aggregate formation. Biogeosciences, *7*, 1007–1015.

Received: *29 April 2014*; revised: *2 September 2014*.